Lithos 308–309 (2018) 196–212

Contents lists available at ScienceDirect

Lithos

journal homepage: www.elsevier.com/locate/lithos

Petrogenesis of Early Cretaceous granitoids from southwest Zhejiang, NE South China Block and its geodynamic implication

Fa-Bin Pan [a,*], Rong Liu [b], Chong Jin [b], Bao-Jian Jia [b], Xiaobo He [c], Zhong Gao [a,d], Lu Tao [a,d], Xiao-Chun Zhou [a,d], Li-Qi Zhang [a,d]

[a] State Key Laboratory of Geological Process and Mineral Resources, China University of Geosciences, Wuhan 430074, PR China
[b] Zhejiang Institute of Geology and Mineral Resource, Hangzhou 310007, PR China
[c] Ocean College, Zhejiang University, Hangzhou 310058, PR China
[d] Faculty of Earth Science, China University of Geosciences, Wuhan 430074, PR China

A R T I C L E   I N F O

Article history:
Received 7 December 2017
Accepted 14 March 2018
Available online 17 March 2018

Keywords:
Early Cretaceous granitoids
Petrogenesis
Temporal-spatial variations
South China Block
Mantle–crust interaction

A B S T R A C T

In situ zircon U–Pb ages, whole-rock major and trace elements, and Sr–Nd isotopic compositions of the Sucun, Yunfeng, and Jingning intrusions from southwest Zhejiang, NE South China Block, are presented to trace their petrogenesis and shed light on its lithosphere evolution. LA–ICP–MS U–Pb zircon dating shows that the Sucun quartz monzonite and Jingning monzogranite were emplaced at ~135 Ma, and the Yunfeng quartz monzonite and Jingning granite were emplaced at 104 and 112 Ma, respectively. All these intrusions are metaluminous to weakly peraluminous and lie within high-K calc-alkaline to shoshonite series field ($SiO_2 = 66–76$ wt%, A/CNK = 0.95–1.09, $K_2O/Na_2O = 0.78–1.77$). The Yunfeng quartz monzonite clearly have lower K_2O and total REE contents, and higher CaO, Na_2O, Al_2O_3, P_2O_5, MgO, and TiO_2 contents, and relatively less enriched Sr–Nd isotopic compositions than those of the Sucun quartz monzonite, indicating that the Yunfeng quartz monzonite were derived from partial melting of a more juvenile lower crust sources compared with the magma source of the Sucun quartz monzonite. The Jingning monzogranite exhibit similar major elements covariations and Nd isotopic compositions, but higher Ba, Sr, and Eu contents and lower Rb, Th, and U contents than those of the Jingning granite. The geochemical features imply that the Jingning monzogranite and granite were fluid-present and fluid-absent anatexis products of the same Paleoproterozoic crustal source, respectively. Whole-rock Sr–Nd isotopic data imply that the estimated amounts of juvenile mantle-derived melts input into the mature crust show southeastward decreasing trend away from the Jiangshan–Shaoxing fault. We propose that roll-back and retreat of the Paleo-Pacific subducting plate might cause extensive asthenosphere mantle upwelling in East China, and the mantle-derived melts tend to rise through the regional main fault zones and preferentially modify the lithosphere nearby these faults.

1. Introduction

Mesozoic–Cenozoic geodynamic evolution of East China is characterized by large scale craton destruction (Fan et al., 2000; Gao, Rudnick, Carlson, Mcdonough, and Liu, 2002; Li et al., 2015; Menzies, 1993; Wu, Walker, Yang, Yuan, and Yang, 2006; Xu, 2001; Zhang, Zhao, Davis, Ye, and Wu, 2014; Zheng et al., 2007, 2015). Coeval magmatic rocks are extensively exposed in East China and adjacent areas (Ho, Chen, Lo, and Zhao, 2003; Wu et al., 2007; Wu, Lin, Wilde, Zhang, and Yang, 2005; Xu, 2014; Zhang et al., 2004; Zhou and Li, 2000), which offer a unique insight into the destruction processes. Although a lot of works have been conducted for deciphering these processes in North China Craton, the timing, mechanisms, and processes are still debated. Two major models have been proposed including thermal–mechanical–chemical erosion and replacement by asthenosphere upwelling (Menzies, 1993; Xu, 2001; Zhang, 2005; Zheng et al., 2007), and delamination of thickened lower continental crust (Gao et al., 2004; Wu et al., 2005). Recent studies emphasized hydro-weakening of the subcontinental lithospheric mantle due to Phanerozoic subducted slab-derived fluids (C. Chen et al., 2016; Hong et al., 2017; Ma et al., 2016; Niu, 2005; Windley, Maruyama, and Xiao, 2010; Zhu et al., 2012).

A few lines of evidences, including source variations of Mesozoic–Cenozoic basalts, variable mantle xenoliths, and heat flow value variations, show that the South China Block lithosphere is heterogeneous and also experienced lithospheric modification (Huang, Su, Zhou, Gao, and Qi, 2017; Liu, Wu, Sun, Chu, and Qiu, 2012; Lu, Zheng, Griffin, and Yu, 2013; X. Li et al., 2014; Xu, Reilly, Griffin, and Zhou, 2000; Zheng et al., 2015). Thus, geological records of the modification processes probably were also preserved in South China Block. Mesozoic granitoids

* Corresponding author.
E-mail address: panfabin@zju.edu.cn (F.-B. Pan).

https://doi.org/10.1016/j.lithos.2018.03.011
0024-4937/

are widespread in Zhejiang, NE South China Block (Chen et al., 2000; Lapierre, Jahn, Charvet, and Yu, 1997; Qiu et al., 2004). Published Nd isotopic data of these Mesozoic granitoids show that the majority of the Triassic granites contain relatively homogeneous compositions of −11 to −15 with T_{2DM} of 2.0 to 2.2 Ga (Li, Ma, Liu, and Robinson, 2012; Mao et al., 2013; Sun, Ma, Liu, and She, 2011; Xu, Hu, Gu, and Lu, 2013; Zhao, Jiang, Chen, Chen, and Ling, 2013), and the Cretaceous granitoids have less enriched and more heterogeneous compositions of −6 to −13 with T_{2DM} of 1.2 to 1.9 Ga (Shen, Ling, Wang, Xu, and Yu, 1999) (Fig. 1a). These features suggest that the Triassic granites were represented reworking of mature crustal materials, while the magma sources for the Cretaceous granitoids have significant input of mantle-derived juvenile materials. However, the temporal-spatial distribution of this modification event and its geodynamical implications remain unclear.

In this paper, we have carried out an integrated study of zircon U–Pb dating combined with Sr–Nd isotopic analyses for four granitoid intrusions from southwest Zhejiang. Our main aims are: (1) to constrain their petrogenesis and secular source evolution in the studied area; (2) to explore the Mesozoic lithospheric modification processes in East China.

2. Geological setting and sampling

East China consists of the North China Craton and the South China Block, separated by the Qinling–Dabie–Sulu Orogenic belt (Fig. 1a). The 2000 km-length NE-SW orientated Jiangshan–Shaoxing (JS) Fault zone divide the South China Block into two major Precambrian continental blocks (Fig. 1a): the Yangtze block in the northwest and the Cathaysia block in the southeast (Li et al., 2009; Li, Li, Li, and Lou, 2008). The southeast Zhejiang, southeast of the JS fault, belongs to the Cathaysia block. The Precambrian basement of this area is composed of the Badu Group (Pt_1) and the Chencai Group (Pt_{2-3}). The Badu Group (Pt_1) and its equivalent the Mayuan Group in north Fujian

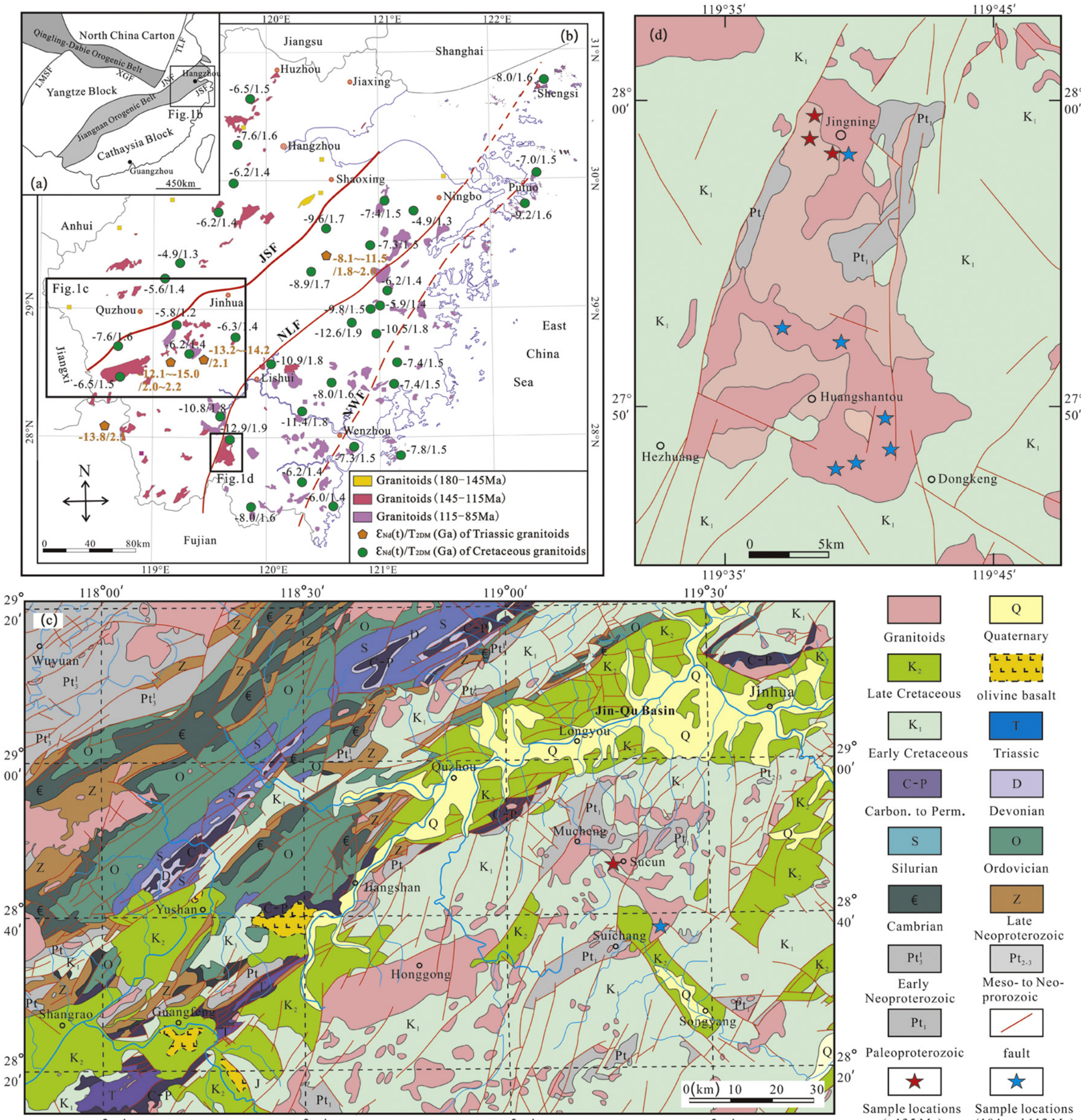

Fig. 1. (a): Tectonic outline of the South China Block showing the study area. JSF: Jiangshan–Shaoxing fault; JNF: Jiangnan fault; TLF: Tan–Lu fault; XGF: Xiangfan–Guangji fault; LMSF: Longmengshan fault. (b): Simplified geological map of the Zhejiang Middle–Late Mesozoic granitoids. The detailed Nd isotopic data sources are from Li et al. (2012), Mao et al. (2013), Sun et al. (2011), Zhao et al. (2013), Xu et al. (2013), Shen et al. (1999). NLF: Ningbo–Lishui fault; NWF: Ninghai–Wenzhou fault. (c): Simplified geological map of the Sucun and Yunfeng quartz monzonite (modified after 1:500,000 regional geological map). (d): Simplified geological map of the Jingning monzogranite and granite (modified after 1:200,000 regional geological map).

are dominantly composed of a series of metamorphic terrestrial clastics, including biotite–plagioclase gneiss, amphibolites, amphibole–plagioclase gneiss, biotite–plagioclase–quartz gneiss, mica schist, and mica–quartz schist (Hu, Xu, Tong, and Chen, 1991). The detritus of the sedimentary protoliths of the Badu Group were considered to be deposited in an arc basin synchronously with ~2.5 Ga volcanism according to the unimodal age distribution (~2.5 Ga) and the positive εHf(t) of its detrital zircons (Yu, Oreilly, Zhou, Griffin, and Wang, 2012). A few granitoids intruded the Badu Group and show Paleoproterozoic emplacement ages (~1.93–1.85 Ma), suggesting that the Badu Group (Pt_1) is a Paleoproterozoic lithostratigraphic unit (Yu et al., 2012; Zhao et al., 2014; Zhao, Zhou, Zhai, Santosh, and Geng, 2015). Besides, SHRIMP U–Pb zircon analysis show that the mafic amphibolites from the Badu Group have crystallization age of 1.77 Ga (Li, 1997), which is coeval with the granitoids magmatism. The Chencai Group ($Pt_{2\text{-}3}$) is mainly composed of gneiss, amphibolite, greenschist and marble (Li et al., 2009; Shui, 1988; Xiao and He, 2005). Origin of this medium- to high-grade metamorphic complex likely represents a relic of Mesoproterozoic to Neoproterozoic island arc (Shui, 1988).

The Precambrian basement of southeast Zhejiang is overlain by widespread Cretaceous volcanic–sedimentary sequences, containing the lower and upper volcanic series (J. Li et al., 2014; Liu, Xu, and Zou, 2012a). The lower volcanic series (K_1: 140–128 Ma), named Moshishan Group, mainly consists of rhyolites, volcaniclastic rocks, and minor basalts, along with minor sandstones, mudstones, and conglomerates in the west region of southeast Zhejiang. The upper volcanic series (K_2: 110–88 Ma) in southeast Zhejiang are named Yongkang Group, Tiantai Group, and Xiaoxiong Group for their distributions in different basins (BGMRZP, 1989). These groups are mainly composed of sandstones, mudstones, and conglomerates with interbedded volcaniclastic rocks, rhyolites, and minor basalts.

Extensive Mesozoic granitoids crop out the Zhejiang Province (Fig. 1b). Most of these rocks were emplaced during ~145 to 85 Ma (Fig. 1b), which show a continent-ward aging trend from east to west (C.-H. Chen et al., 2016; Chen et al., 2000; Liu, Qiu, and Zhao, 2016; P. Li et al., 2013; Qiu et al., 2004; Wong et al., 2011; Z. Li et al., 2013; Zhao, Qiu, Liu, and Wang, 2016). These rocks include both of I-type and A-type granites. Generation of I-type granites is usually attributed to the Paleo-Pacific plate subduction, whereas the development of A-type granites may indicate occurrence of an extensional environment in South China Block (Lapierre et al., 1997; Qiu et al., 2004; Wong et al., 2009; Z. Li et al., 2013). Recently, a few Triassic alkaline granitoids were also found in central to southwest Zhejiang province (Mao et al., 2013; Sun et al., 2011; Zhao et al., 2013).

This study is conducted in southwest Zhejiang province (Fig. 1b). Two granitoid intrusions from northeast Suichang city and two granitoid intrusions from Jingning city have been sampled for this study (Fig. 1c and d). Most of the collected samples are fresh, without visible alteration (Fig. 2a–h). A few samples from Jingning granite show slight chloritization (Fig. 2i).

The Sucun quartz monzonite (5.8 km^2) is located at Sucun (Fig. 1c). It is sharp contact with its wall-rocks (Badu Group and Moshishan Group). The quartz monzonite is porphyritic with minerals of K-feldspar, plagioclase, quartz, and minor amphibole and biotite

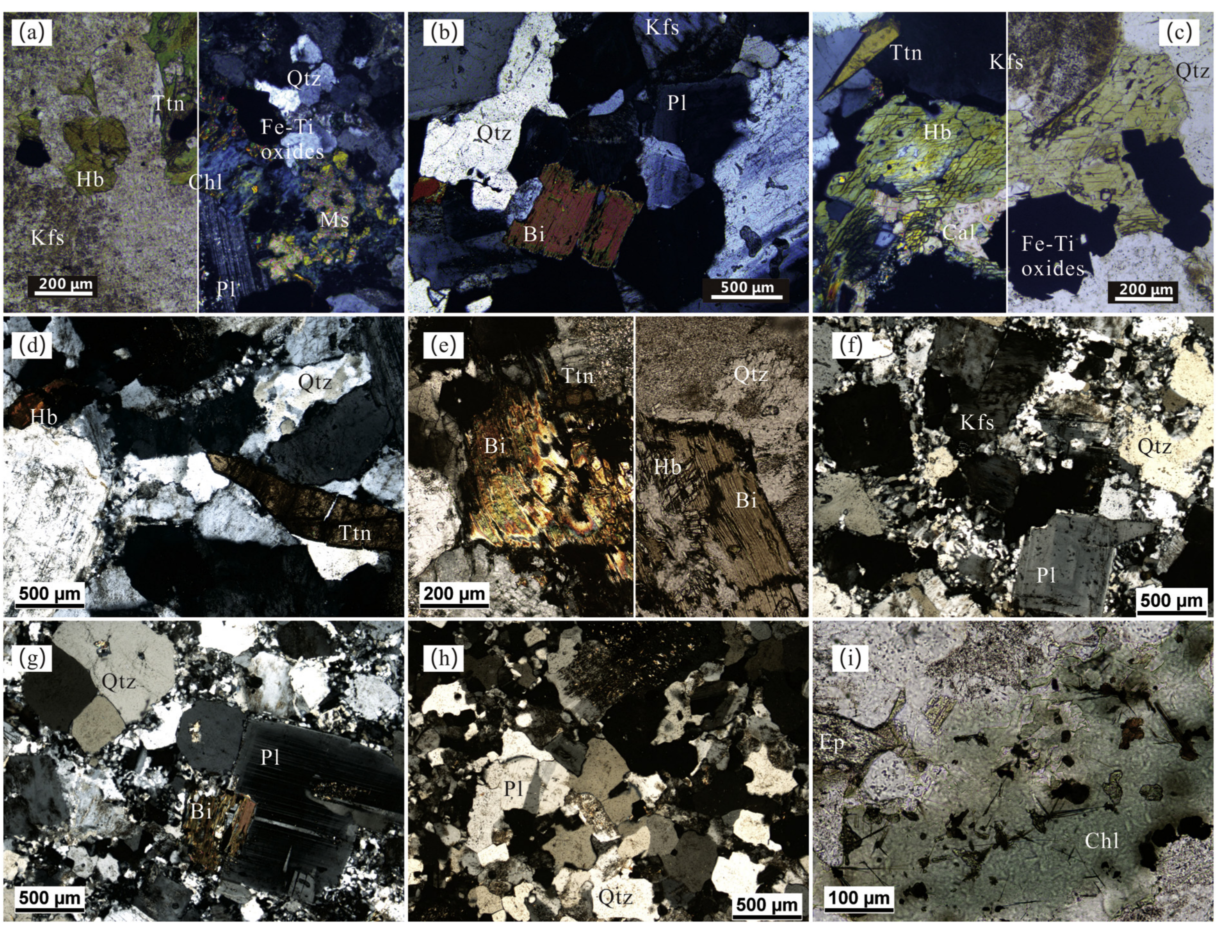

Fig. 2. (a): microphotograph of the Sucun quartz monzonite (The left side: plane polarized light, the right side: perpendicular polarized light). (b) and (c): microphotograph of the Yunfeng quartz monzonite (The left side: perpendicular polarized light, the right side: plane polarized light for (c)). (d) and (e): microphotographs of the Jingning monzogranite (The left side: perpendicular polarized light, the right side: plane polarized light for (e)). (f), (g), (h) and (i): microphotographs of the Jingning granite. Hb: hornblende; Bi: biotite; Qtz: quartz; Kfs: K-feldspar; Pl: plagioclase; Ttn: titanite; Ep: epidote; Chl: chlorite.

(commonly 2–6 mm in length, with minor 8–20 mm) which form 65–70 vol% of the bulk rock; the matrix (grain size 0.15–0.3 mm) contains the similar mineral compositions (Fig. 2a). Overall, the porphyritic quartz monzonite comprises quartz (~25 vol%), plagioclase (~30 vol%), K-feldspar (~35 vol%), hornblende (~5 vol%) and biotite (~3 vol%), with accessory zircon, titanite, apatite, monazite and Fe–Ti oxides. Mafic magmatic enclaves (MME) (10–20 cm in length) are abundant in the quartz monzonite. Typical modal compositions for the enclaves are plagioclase (~30–40 vol%), hornblende (~50–60 vol%) and biotite (~0–5 vol%) (BGMRZP, 1989). The MME occur as lenses with sharp contacts against the host quartz monzonite.

The Yunfeng quartz monzonite, intruded into the Moshishan Group, is located ~10 km northeast of the Suichang city (Fig. 1c). It is medium-grained and mainly contains quartz (~20 vol%), plagioclase (30–35 vol%), K-feldspar (35–40 vol%), hornblende (~5 vol%), and biotite (~5 vol%), with minor accessory minerals such as zircon, apatite, titanite and Fe–Ti oxides (Fig. 2b and c). MME (10–20 cm in length) with spheroidal to ellipsoidal shape are also abundant in this quartz monzonite.

The Jingning pluton (>200 km^2 in outcrop area), located near the Ningbo–Lishui fault (Fig. 1b), mainly consists of massive monzogranite and granite (Fig. 1d). The medium-grained Jingning monzogranite is mainly composed of quartz (30–40 vol%), plagioclase (20–25 vol%), K-feldspar (25–35 vol%), biotite (~3 vol%) (Fig. 2d and e). Minor hornblende is sometimes present as reaction remnant (Fig. 2e). Zircon, apatite, titanite, and Fe–Ti oxides are present as accessories. The Jingning granite is porphyritic with minerals of plagioclase, quartz, and minor biotite (commonly 1–3 mm in length) which form 70 vol% of the bulk rock; the matrix (grain size 0.1–0.3 mm) mainly contains quartz and K-feldspar (Fig. 2f, g, and h). Overall, the porphyritic granite comprises quartz (45–55 vol%), plagioclase (15–20 vol%), K-feldspar (25–35 vol %), hornblende (~5 vol%) and biotite (~3 vol%), with accessory zircon, titanite, apatite, monazite and Fe–Ti oxides.

3. Analytical methods

Whole-rock samples were analyzed for major elements, using a Shimadzu sequential X-ray fluorescence spectrometer (XRF–1800) at the State Key Laboratory of Geological Processes and Mineral Resources (GPMR), China University of Geosciences, Wuhan. Loss on ignition (LOI) was determined by weight loss after drying at 1000 °C. The results obtained from Chinese national standards and repeated samples show analytical uncertainties of the XRF data of ~1 % for element contents >10 wt% and ~5% for element contents <1.0 wt%. More details about the analytical procedure for the two labs have been described in Ma et al. (2012). The analytical uncertainty is generally <5%. Trace elements, including REE, were measured using Agilent 7500a ICP–MS at GPMR. The detailed sample-digesting procedure for ICP–MS analysis and analytical precision and accuracy see Liu, Zong, Kelemen, and Gao (2008) and Zhang, Liu, Ling, and Gao (2017).

Whole-rock Sr and Nd isotopic ratios were measured by a Triton thermal ionization mass spectrometer at GPMR. $^{87}Rb/^{86}Sr$ and $^{147}Sm/^{144}Nd$ ratios were calculated from measured Rb, Sr, Sm and Nd contents by ICP–MS. The measured Sr and Nd isotopic ratios were normalized to $^{86}Sr/^{88}Sr = 0.1194$ and $^{146}Nd/^{144}Nd = 0.7219$, respectively. During the period of analysis, NBS987 standard yielded an average $^{87}Sr/^{86}Sr$ value of 0.710239 ± 10 (2σ) and BCR-2 standard gave an average $^{143}Nd/^{144}Nd$ value of 0.512620 ± 2 (2σ). For details of the Sr and Nd isotopic analytical procedures are the same as description by Gao et al. (2004) and Zhang et al. (2017).

U–Pb zircon dating was also conducted by LA–ICP–MS at GPMR. Zircon 91500 was used as external standard for U–Pb dating, and was repeatedly analyzed every 5 analyses. Time-dependent drifts of U–Th–Pb isotopic ratios were corrected using a linear interpolation (with time) for every five analyses according to the variations of 91500 (i.e., 2 zircon 91500 + 5 samples + 2 zircon 91500) (Liu et al., 2010). Preferred U–Th–Pb isotopic ratios used for zircon 91500 are from Wiedenbeck et al. (1995). The uncertainties of preferred values for the external standard 91500 were propagated to the combined errors of the samples. Concordia diagrams and weighted mean calculations were made using Isoplot/Ex_ver3 (Ludwig, 2003).

4. Results

4.1. U–Pb zircon ages

LA–ICP–MS zircon U–Pb data are listed in the Appendix Table A1, and representative zircon CL images and their U–Pb concordia plots are shown in Fig. 3. In CL images, all of the analyzed zircons exhibit oscillatory zoning (Fig. 3), indicating a magmatic origin (Corfu, Hanchar, Hoskin, and Kinny, 2003).

4.1.1. Sucun quartz monzonite (SC05)

Twenty U–Pb isotopic analyses from 20 zircon grains were obtained from sample SC05. All zircons are euhedral with grain length of 150–300 μm and aspects ratios of 2:1–4:1. These analyses have variable U (151–1265 ppm) and Th (154–1168 ppm) with high Th/U ratios of 0.57–1.14. Nineteen analyses yield $^{206}Pb/^{238}U$ ages between 129.7 ± 1.6 Ma and 140.4 ± 2.6 Ma, with a weighted mean of 136.1 ± 1.1 Ma (MSWD = 1.6) (Fig. 3a), representing the magma crystallization age of the Sucun biotite granite. One additional analysis gives $^{206}Pb/^{238}U$ ages of 151.6 ± 3.6 Ma, that could represent a captured grain.

4.1.2. Yunfeng quartz monzonite (YF-02)

The zircon grains from sample YF-02 are euhedral, transparent, and show short prismatic forms (200–300 μm long) with aspects ratios of 3:1–4:1. They have low U (139–595 ppm) and Th (71–693 ppm) values with Th/U ratios of 0.12–2.27. Eighteen analyses yield $^{206}Pb/^{238}U$ ages between 98.6 ± 1.6 Ma and 113.6 ± 2.1 Ma, with a weighted mean of 104.2 ± 1.9 Ma (MSWD = 3.3) (Fig. 3b). Two analyses on inherited cores give $^{207}Pb/^{206}Pb$ ages of 1.8 Ga, which are consistent with the age of the magmatic rocks from Badu Group.

4.1.3. Jingning monzogranite (JNHX-26)

Zircons from the Jingning monzogranite (JNHX-26) are colorless, transparent and euhedral. The zircons have 100 to 150 μm in length with aspects ratios of 3:1–4:1. The analyzed grains have variable U (32–2445 ppm) and Th (35–2361 ppm) with high Th/U ratios of 0.44–4.08 (Appendix Table A1). Nineteen analyses on zircon crystals yield $^{206}Pb/^{238}U$ ages between 129.7 ± 2.2 Ma and 149.5 ± 2.8 Ma, with a weighted mean of 134.6 ± 2.8 Ma (MSWD = 7.5) (Fig. 3c), representing the magma crystallization age of the Jingning monzogranite.

4.1.4. Jingning granite (JNHX-09)

Zircons from the Jingning granite (JNHX-09) are euhedral, with crystal length of 200 to 400 μm in length with aspects ratios of 2:1–5:1. Thirteen analyses, containing U contents of 186–1476 ppm and Th contents of 131–1170 ppm with Th/U ratios of 0.50–1.78, yield $^{206}Pb/^{238}U$ ages between 106.0 ± 2.4 Ma and 115.7 ± 1.8 Ma, with a weighted mean of 112.3 ± 1.9 Ma (MSWD = 3.7) (Fig. 3d), representing the magma crystallization age of the Jingning granite. Two additional analyses give $^{206}Pb/^{238}U$ ages of 141 and 145 Ma, which could represent captured grains. One grain showing relatively high U (1807 ppm) and Th (633 ppm), yield younger $^{206}Pb/^{238}U$ ages between 94.7 ± 2.0 Ma (Fig. 3d), which we infer to be due to radiogenic lead loss.

4.2. Major and trace elements

Major and trace elements data of all samples are given in Table 1. They are described in two groups corresponding to their spatial distribution relationships.

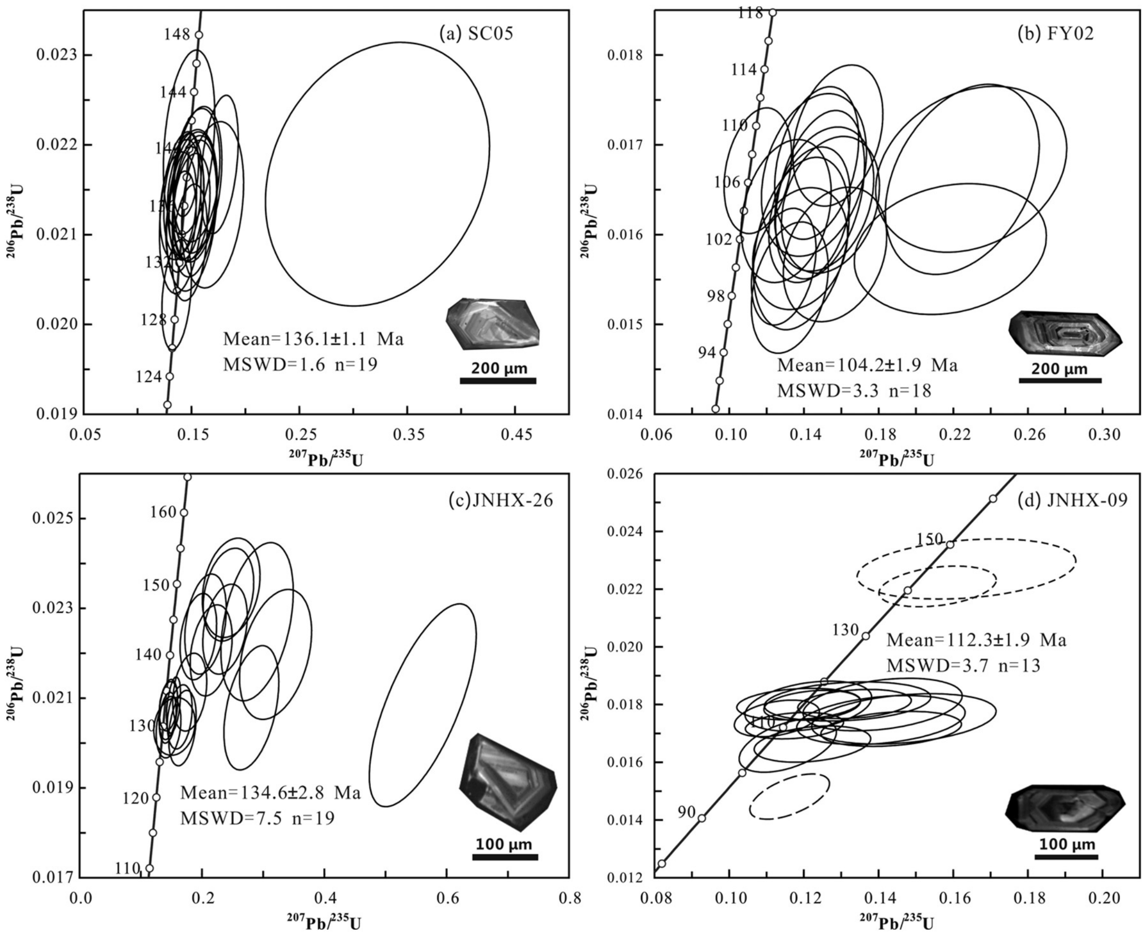

Fig. 3. U–Pb Tera-Wasserburg plots for U–Pb zircon analyses and representative CL images for zircons from samples SC05, YF02, JNHX-26, and JNHX-09.

4.2.1. The Sucun and Yunfeng quartz monzonite

The Sucun quartz monzonite show $SiO_2 = 67.7–68.9$ wt%, $Al_2O_3 = 14.7–15.8$ wt%, $K_2O = 5.13–5.41$ wt% and $K_2O/Na_2O = 1.35–1.47$, with A/CNK ratios of 0.99–1.01, indicating that they are all weakly peraluminous and lying within the shoshonite series field (Fig. 4). Besides, they have CaO of 1.57–1.88 wt%, MnO of 0.06–0.09 wt%, TiO_2 of 0.44–0.48 wt%, Fe_2O_3 of 3.24–3.57 wt%, MgO of 0.68–0.74 wt% with Mg# of 32–34 (Table 1). The Yunfeng quartz monzonite show slightly lower SiO_2 (66.0–67.9 wt%) and K_2O (3.98–4.32 wt%) contents and K_2O/Na_2O ratios (0.78–1.05), higher CaO (1.73–2.87 wt%), Na_2O (4.13–5.19 wt%), Al_2O_3 (15.73–16.05 wt%), P_2O_5 (0.19–0.22 wt%), TiO_2 (0.51–0.58 wt%), MgO (1.09–1.19 wt%) and Mg# (43–45) than those of the Sucun quartz monzonite (Table 1 and Fig. 5). The Sucun and Yunfeng quartz monzonites have similar Fe_2O_3 and MnO contents.

In the trace element spider diagram (Fig. 6a), all the samples from the Sucun and Yunfeng quartz monzonites exhibit enrichment of Rb, Th, and Pb values, and negative Ba and HFSEs (e.g. Nb, Ta, P, and Ti) anomalies. In the Chondrite-normalized REE pattern (Fig. 6c), the Sucun quartz monzonite display fractionated REE patterns with $(La/Yb)_N$ ratios of 15.92–18.59, and clearly negative Eu anomalies ($Eu/Eu^* = 0.43–0.54$). The Yunfeng quartz monzonite contain obviously lower REE contents (except Eu values) than those of the Sucun quartz monzonite (Fig. 6c), although they display similar REE fractionation ($(La/Yb)_N = 16.98–19.80$) with slightly negative Eu anomalies ($Eu/Eu^* = 0.74–0.83$).

4.2.2. The Jingning monzogranite and granite

Three samples from the Jingning monzogranite have SiO_2 contents of 69.8–75.2 wt%. The Jingning granites have slightly higher SiO_2 contents (72.8–76.4 wt%). All the samples from the Jingning monzogranite and granite show comparable K_2O (3.90–5.39 wt%) and Na_2O (3.40–4.03 wt%), CaO (0.76–2.51 wt%), Al_2O_3 (12.82–15.20 wt%) with K_2O/Na_2O ratios of 1.03–1.77 and A/CNK ratios of 0.99–1.09 (Table 1), indicating that they are metaluminous to weakly peraluminous and lying within the high-K calc-alkaline series field (Fig. 4). Both the Jingning monzogranite and granite show similar covariations between Fe_2O_3 (0.62–2.95 wt%), MgO (0.13–0.95 wt%), P_2O_5 (0.02–0.14 wt%), TiO_2 (0.10–0.47 wt%) and SiO_2 contents (Fig. 5).

All the Jingning monzogranite and granite show enrichment of LILEs and negative anomalies of HFSEs in the primitive-mantle-normalized trace element patterns (Fig. 6b). The Jingning monzogranite have obviously higher Ba (986–1944 ppm), Sr (468–1145 ppm), Eu (1.38–1.67 ppm), and Zr (158–306 ppm) contents and lower Rb (59–126 ppm), Th (4.41–15.2 ppm), and U (0.96–2.82 ppm) contents than those of the Jingning granite (Fig. 6b). Besides, the Jingning monzogranite are also characterized by higher Sc (7.3–20.5 ppm), V (25–182 ppm), Cr (0.63–30.80 ppm), Ni (1.88–12.20 ppm), Cu (1.82–28.2 ppm), and Zn (58–90 ppm) contents and lower Co (53–92 ppm) contents compared with those of the Jingning granite (Table 1). The Jingning monzogranite display clearly fractionated REE patterns with $(La/Yb)_N$ ratios of 4.88–17.51 with slightly negative Eu anomalies ($Eu/Eu^* = 0.72–0.85$) in the Chondrite-normalized REE pattern (Fig. 6d). The Jingning granite are featured by negative Eu anomalies ($Eu/Eu^* = 0.23–0.67$) and slightly increasing HREE pattern ($Dy_N/Yb_N = 0.71–1.20$) (Table 1).

4.3. Sr–Nd isotopes

Whole-rock Rb–Sr and Sm–Nd isotopic data for the studied granitoids are listed in Table 2. For all samples, their initial $^{87}Sr/^{86}Sr$ isotopic

Table 1
Major oxides and trace elements for the granitoids in SW Zhejiang Province, NE South China Block.

Sample No.	SC-01	SC-04	SC-05	SC-06	YF-01	YF-02	YF-03	YF-04	YF-05	JNHX20	JNHX25	JNHX26	JNHX01	JNHX02	JNHX09	JNHX12	JNHX13	JNHX14	JNHX18
Lithology	Sucun quartz monzonite				Yunfeng quartz monzonite					Jingning monzogranite			Jingning granite						
Major elements (wt%)																			
SiO_2	68.11	67.71	68.93	68.35	66.00	67.89	66.51	67.20	67.01	71.54	69.80	75.19	74.73	76.43	76.27	72.75	76.28	75.71	73.16
TiO_2	0.47	0.48	0.44	0.45	0.55	0.51	0.54	0.55	0.58	0.47	0.39	0.15	0.15	0.11	0.12	0.23	0.14	0.10	0.26
Al_2O_3	14.67	14.79	14.75	15.03	15.78	16.04	16.05	15.73	16.02	13.81	15.20	13.20	13.45	12.82	13.02	14.29	13.23	13.40	13.79
Fe_2O_3	3.57	3.43	3.36	3.24	3.39	3.07	3.47	3.59	3.49	2.95	2.75	1.32	1.42	1.10	1.01	1.87	1.03	0.62	2.14
MnO	0.08	0.06	0.09	0.06	0.03	0.08	0.11	0.12	0.09	0.05	0.08	0.06	0.06	0.03	0.05	0.08	0.06	0.04	0.06
MgO	0.74	0.74	0.68	0.71	1.10	1.09	1.16	1.19	1.19	0.55	0.95	0.20	0.27	0.15	0.17	0.49	0.22	0.13	0.63
CaO	1.57	1.63	1.88	1.69	1.73	2.59	2.87	2.68	2.77	1.57	2.51	0.81	1.21	0.91	0.93	1.69	0.98	0.76	1.91
Na_2O	3.79	3.73	3.63	3.67	5.19	4.13	4.37	4.13	4.16	3.05	3.52	4.03	3.76	3.50	3.58	3.71	3.40	3.52	3.78
K_2O	5.13	5.41	5.13	5.38	4.04	3.98	4.14	4.32	4.13	5.39	4.25	4.71	4.60	4.70	4.72	4.36	4.41	4.81	3.90
P_2O_5	0.15	0.16	0.14	0.14	0.20	0.19	0.20	0.21	0.22	0.13	0.14	0.03	0.04	0.02	0.03	0.07	0.03	0.02	0.09
LOI	1.72	1.85	0.99	1.28	2.01	0.43	0.57	0.28	0.35	0.51	0.41	0.30	0.30	0.23	0.10	0.46	0.22	0.94	0.28
Total	100.00	99.99	100.02	100.00	100.02	100.00	100.00	99.99	100.00	100.01	99.99	100.00	100.00	100.00	99.99	100.00	100.00	100.05	100.00
A/CNK	1.00	0.99	0.99	1.01	0.98	1.01	0.95	0.96	0.98	1.01	1.02	1.00	1.01	1.03	1.03	1.03	1.09	1.08	0.99
Mg#	33	33	32	34	43	45	44	44	44	30	45	26	31	24	28	38	33	33	41
K_2O/Na_2O	1.35	1.45	1.41	1.47	0.78	0.96	0.95	1.05	0.99	1.77	1.21	1.17	1.22	1.34	1.32	1.18	1.30	1.37	1.03
Trace elements (ppm)																			
Li	32.04	22.43	20.23	13.62	24.65	14.79	16.78	16.71	12.81	16.67	14.43	15.86	12.38	8.47	20.00	14.59	17.86	22.38	9.02
Be	3.31	3.12	3.18	2.93	2.35	2.54	2.46	2.40	2.26	3.19	2.08	1.59	3.42	4.02	2.70	5.17	3.43	4.09	4.70
Sc	6.28	6.97	7.03	6.17	4.38	5.02	4.43	4.44	4.55	7.27	12.85	20.53	2.17	1.69	3.27	2.18	3.06	3.92	1.80
V	20.61	23.78	20.72	18.49	43.13	46.83	46.23	46.81	43.83	24.78	107.24	182.02	7.41	5.30	17.81	6.03	11.95	13.97	6.75
Cr	1.41	1.69	1.28	1.51	2.35	3.52	2.93	3.58	3.74	0.63	14.49	30.79	0.72	0.55	0.90	0.63	0.61	0.62	0.52
Co	99.6	71.9	62.5	80.8	42.7	76.0	93.7	103.1	90.3	91.8	52.9	54.5	127.2	135.9	122.9	145.3	114.8	129.1	104.8
Ni	2.25	2.01	1.98	1.81	2.44	3.32	3.81	4.55	3.92	1.88	9.30	12.22	2.07	1.99	2.66	2.38	1.91	2.28	1.87
Cu	1.75	1.98	2.35	2.54	2.53	5.13	4.43	4.87	6.28	1.82	9.80	28.15	6.82	1.44	1.45	2.60	1.29	1.45	7.94

(continued on next page)

Table 1 (*continued*)

Sample No.	SC-01	SC-04	SC-05	SC-06	YF-01	YF-02	YF-03	YF-04	YF-05	JNHX20	JNHX25	JNHX26	JNHX01	JNHX02	JNHX09	JNHX12	JNHX13	JNHX14	JNHX18
Lithology	Sucun quartz monzonite				Yunfeng quartz monzonite					Jingning monzogranite			Jingning granite						
Zn	51.87	49.60	42.24	51.68	28.26	75.28	49.18	53.65	51.77	57.96	72.26	90.33	16.87	6.22	23.08	14.53	19.96	36.60	10.63
Ga	17.85	18.42	18.50	17.73	17.61	18.51	18.67	17.98	18.03	19.50	20.54	19.74	13.86	14.11	14.75	14.09	15.17	16.11	14.24
Rb	184.2	182.8	194.1	191.2	141.3	148.0	133.5	152.6	143.9	125.7	76.0	58.8	182.8	257.5	153.9	275.3	190.8	182.9	234.0
Sr	242.2	236.3	235.0	253.9	374.3	635.9	647.7	652.9	646.9	468.1	1145.3	856.1	149.7	81.6	311.1	88.2	311.5	193.1	127.5
Y	34.46	36.14	37.08	31.45	19.38	19.92	20.42	19.15	19.12	29.28	23.85	26.69	23.31	34.52	18.09	40.40	22.32	30.86	29.58
Zr	265	279	273	247	221	204	205	205	206	306	199	158	111	92	134	100	149	179	111
Nb	20.01	21.13	21.24	17.53	16.63	17.13	17.25	17.08	17.26	17.19	12.06	10.25	14.65	22.31	13.45	21.28	12.20	19.53	21.63
Cs	3.97	3.51	3.18	2.75	2.24	2.29	2.48	2.47	2.54	2.71	1.83	5.99	2.54	1.61	1.65	5.57	2.37	2.42	2.29
Ba	897	851	770	957	1056	1034	998	1148	1255	1681	1944	986	471	150	804	180	1078	394	261
La	75.24	77.74	75.68	74.33	50.42	52.35	48.48	48.48	46.79	60.85	34.61	26.68	37.38	27.47	46.92	21.96	50.58	56.31	19.66
Ce	136.0	141.9	138.2	133.8	89.5	92.0	90.0	87.1	86.5	115.2	68.2	54.6	62.8	50.9	80.1	42.9	85.1	98.09	36.36
Pr	14.83	15.39	15.09	14.48	9.59	9.91	9.95	9.46	9.36	12.61	7.92	6.60	6.62	5.67	7.86	4.79	8.35	10.02	4.06
Nd	53.46	56.74	54.71	51.76	34.88	36.04	36.60	34.42	34.13	45.40	30.44	26.91	22.41	20.71	25.22	17.55	27.88	33.48	15.02
Sm	9.23	9.89	10.04	8.85	5.79	5.83	5.96	5.57	5.47	7.89	5.61	5.33	4.22	4.80	3.85	4.12	4.47	5.89	3.45
Eu	1.38	1.39	1.29	1.42	1.32	1.36	1.30	1.25	1.33	1.67	1.44	1.38	0.50	0.35	0.76	0.38	0.81	0.59	0.40
Gd	7.07	7.52	7.79	6.68	4.16	4.24	4.42	4.03	3.99	5.85	4.47	4.80	3.51	4.35	2.87	4.23	3.45	4.66	3.43
Tb	1.09	1.15	1.18	1.00	0.60	0.61	0.63	0.58	0.58	0.88	0.68	0.72	0.57	0.77	0.44	0.77	0.52	0.76	0.63
Dy	6.20	6.75	6.93	5.85	3.36	3.56	3.63	3.31	3.33	4.92	3.92	4.44	3.45	4.92	2.62	5.05	3.28	4.51	4.08
Ho	1.18	1.28	1.32	1.11	0.65	0.66	0.68	0.64	0.63	0.96	0.76	0.88	0.73	1.06	0.51	1.07	0.65	0.95	0.86
Er	3.35	3.50	3.62	3.02	1.86	1.91	1.93	1.86	1.82	2.73	2.18	2.52	2.24	3.24	1.52	3.50	1.97	2.75	2.74
Tm	0.50	0.51	0.55	0.43	0.27	0.29	0.29	0.28	0.29	0.41	0.34	0.42	0.37	0.57	0.27	0.66	0.37	0.48	0.49
Yb	3.20	3.35	3.41	2.87	1.83	1.93	1.97	1.89	1.98	2.75	2.35	2.59	2.68	4.04	1.92	4.79	2.47	3.30	3.54
Lu	0.48	0.47	0.52	0.41	0.28	0.30	0.30	0.28	0.30	0.41	0.34	0.38	0.42	0.67	0.30	0.74	0.38	0.51	0.57
Hf	7.23	7.48	7.40	6.78	5.73	5.44	5.47	5.52	5.58	6.78	5.11	3.98	3.60	3.70	3.84	3.65	4.02	5.28	3.81
Ta	1.56	1.41	1.46	1.33	1.27	1.42	1.43	1.53	1.63	1.24	0.89	0.67	1.92	2.76	1.59	3.25	1.53	1.96	2.25
Tl	0.92	0.83	0.84	0.92	0.78	0.83	0.71	0.87	0.83	0.82	0.46	0.39	0.92	1.14	0.68	1.09	0.94	0.79	1.45
Pb	27.73	23.62	23.19	35.09	10.21	27.62	30.56	27.10	26.21	26.83	15.32	11.59	19.90	18.06	16.42	20.96	15.60	15.50	15.45
Th	25.69	24.30	25.51	21.87	20.24	21.78	20.32	23.68	24.27	15.20	6.64	4.41	19.04	28.12	28.04	25.73	15.79	23.49	27.78
U	3.95	3.72	3.86	2.82	4.10	4.14	4.01	3.37	3.89	2.82	1.08	0.96	4.22	7.32	6.10	8.55	3.82	4.43	4.29
La_N/Yb_N	16.89	16.66	15.92	18.59	19.80	19.49	17.61	18.42	16.98	9.99	4.88	17.51	3.29	14.71	12.23	3.99	15.85	10.58	7.39
Dy_N/Yb_N	1.30	1.35	1.36	1.37	1.23	1.24	1.23	1.18	1.13	0.86	0.82	0.91	0.71	0.89	0.91	0.77	1.20	1.12	1.15
Eu/Eu*	0.50	0.47	0.43	0.54	0.78	0.80	0.74	0.77	0.83	0.72	0.85	0.82	0.39	0.23	0.67	0.28	0.60	0.33	0.35
Rb/Sr	0.76	0.77	0.83	0.75	0.38	0.23	0.21	0.23	0.22	0.27	0.07	0.07	1.22	3.16	0.49	3.12	0.61	0.95	1.83

Notes: Mg# = molar (MgO / (MgO + FeOt)) ∗ 100; A/CNK = molar Al_2O_3 / (CaO + Na_2O + K_2O).

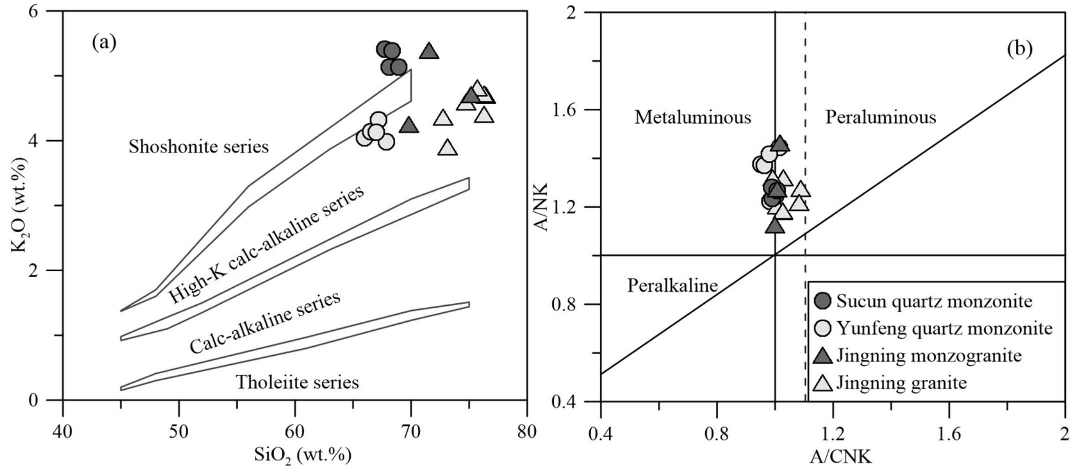

Fig. 4. K_2O versus SiO_2 diagram (a) and A/NK [molar ratio Al_2O_3 / (Na_2O + K_2O)] versus A/CNK [molar ratio Al_2O_3 / (CaO + Na_2O + K_2O)] diagram (b) for the Sucun and Yunfeng quartz monzonites, and the Jingning monzogranite and granite.

ratio (I_{Sr}) and $\varepsilon_{Nd}(t)$ values are calculated at their crystallization ages (Table 2). The Sucun quartz monzonite have I_{Sr} ratios of 0.7085 to 0.7089 and negative $\varepsilon_{Nd}(t)$ values of −8.17 to −8.07 with T_{2DM} of 1.6 Ga. For the Yunfeng quartz monzonite, five samples show slightly lower I_{Sr} ratios of 0.7081 to 0.7085 and higher $\varepsilon_{Nd}(t)$ value of −5.32 to −4.85 with T_{2DM} of 1.3 Ga. The Jingning monzogranite and granite

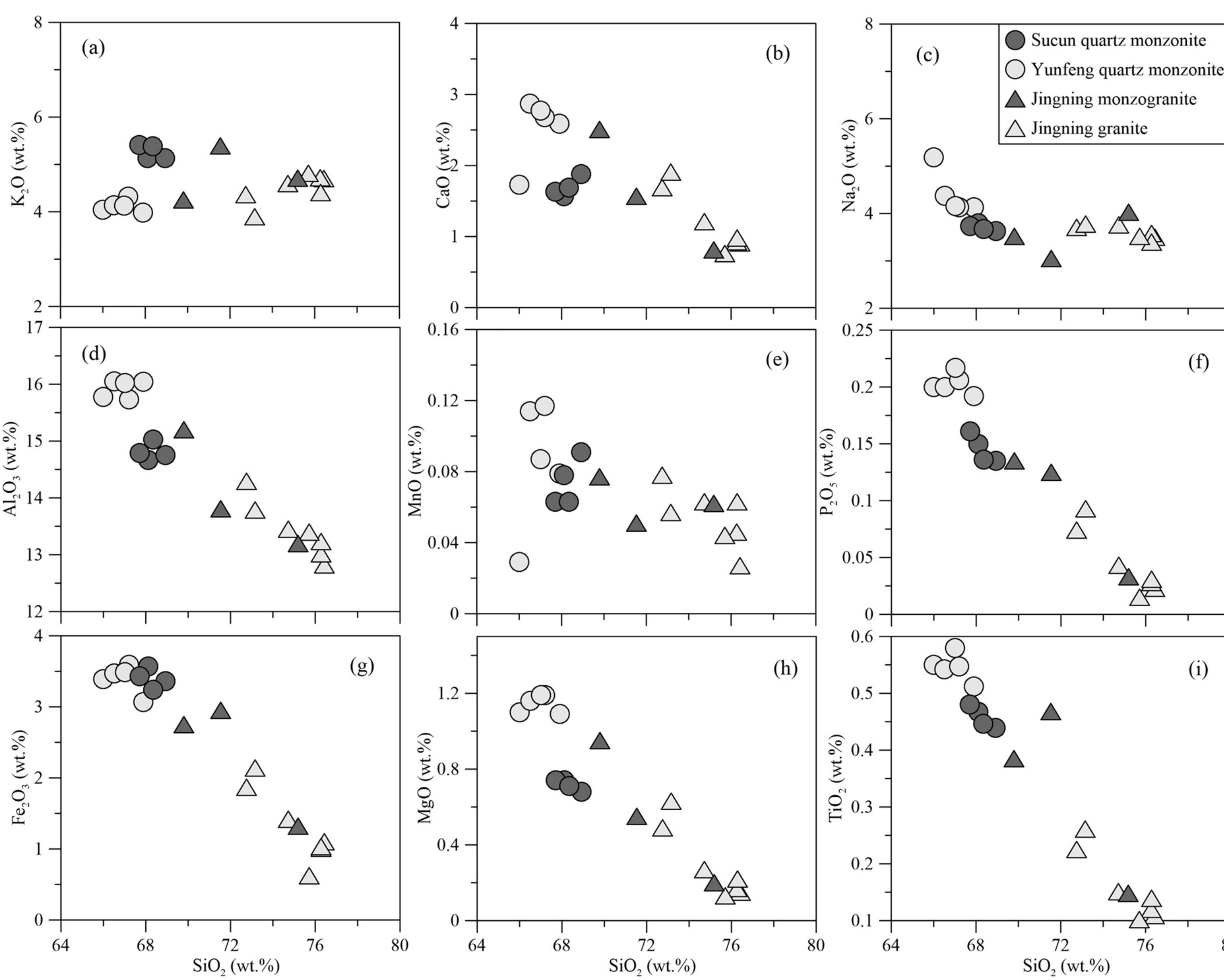

Fig. 5. Harker diagrams for the Sucun and Yunfeng quartz monzonites, and the Jingning monzogranite and granite.

exhibit variable I_{Sr} ratios of 0.6977–0.7345, probably due to their variable $^{87}Rb/^{86}Sr$ ratios (Table 2). They show similar Nd isotopic composition ($\varepsilon_{Nd}(t) = -11.51$ to -8.11 and T_{2DM} of 1.6–1.9 Ga).

5. Discussion

5.1. Petrogenesis

5.1.1. The Sucun and Yunfeng quartz monzonite

Mafic enclaves are present in both the Sucun and Yunfeng quartz monzonites, indicating mantle-derived melts locally contributed in the geochemical features of these quartz monzonites (Liu, Qiu, Li, and Li, 2012b; Liu, Qiu, Zhao, and Yang, 2014b). However, all the samples in this study were collected far away from the mafic enclaves for minimizing the mantle-source contribution. They contain low MgO (0.71–1.19 wt%), Cr (1.28–3.74 ppm), and Ni (1.81–4.55 ppm) contents with Mg# values of 32–45 (Table 1), indicating low mantle-derived melts influence. Major and trace elements of both these two quartz monzonites show relatively homogeneous and irrelevant patterns (Figs. 5, 6a, and 7). Besides, Sr–Nd isotopic compositions are also homogeneous (Table 2). Thus, all of these features are consistent with insignificant mantle-derived melts contribution, and the geochemical compositions of the Suncun and Yunfeng quartz monzonite are dominantly resulted from partial melting of their magma sources and the following modification during magma emplacement.

The Sucun and Yunfeng quartz monzonites contain relatively homogeneous SiO_2 (66.0–68.9 wt%) with metaluminous to weakly peraluminous (A/CNK = 0.95–1.01) (Table 1). Hornblende and titanite are present in both these intrusions (Fig. 2a–c). These features together indicate that they belong to I-type granitoids which were derived from igneous sources in the crust (Chappell, 1999; Chappell and White, 1992). The lower and middle crust are commonly considered to be dry, and partial melting of crustal materials results from dehydration of amphibole and biotite with peritectic minerals of orthopyroxene, clinopyroxene, garnet, and plagioclase (Patiño Douce, 1999; Rapp and Watson, 1995; Weinberg and Hasalova, 2015). The relatively constant FeO contents of the Sucun and Yunfeng quartz monzonite (Fig. 8a) are tightly related to dehydration melting of dry magma sources (Weinberg and Hasalova, 2015). Amphibole-dominated sources commonly contain more ferromagnesian contents than those of biotite-dominated sources. Thus, melts generated by amphibole-dehydration partial melting have wide total abundances of $Al_2O_3 + FeO + MgO + TiO_2$ with restricted range of $Al_2O_3 / (FeO + MgO + TiO_2)$ ratios (Patiño Douce, 1999). The high $Al_2O_3 + FeO + MgO + TiO_2$ contents and restricted ranges of $Al_2O_3 / (FeO + MgO + TiO_2)$ ratios of the analyzed samples indicate dehydration melting of amphibole (Fig. 8b). Weakly negative Eu anomalies (Eu/Eu* = 0.43–0.83) and moderate Sr contents (235–647 ppm) for the Sucun and Yunfeng quartz monzonite suggest that plagioclase may be present in the residuum.

The Sucun quartz monzonite exhibit I_{Sr} ratios of 0.7085–0.7089 and $\varepsilon_{Nd}(t)$ values of -8.17 to -8.07 with T_{2DM} of 1.6 Ga, indicating they were derived from the mature lower crust of our study area. Thus, amphibolite from the Paleoproterozoic Badu Group might be dominantly their magma sources which represent the most mature crustal materials in this area. Two-stage crustal model ages (1.6 Ga) of the Sucun quartz monzonite are slightly younger than the Badu Group (≥1.93–1.85 Ma) (Yu et al., 2012; Zhao et al., 2014, 2015). This feature suggests that the magma source of the Sucun quartz monzonite has likely been slightly modified by the mantle-derived juvenile material.

Two inherited zircon cores, giving $^{207}Pb/^{206}Pb$ ages of 1.8 Ga, suggest that the Badu Group may also be the dominated magma source for the Yunfeng quartz monzonite. The Yunfeng quartz monzonite show lower I_{Sr} ratios (0.7081–0.7085) and higher $\varepsilon_{Nd}(t)$ values (-5.32 to -4.85) with more juvenile T_{2DM} (1.3 Ga), compared with those of the Sucun quartz monzonite. Besides, the Yunfeng quartz monzonite have higher MgO, TiO_2, Na_2O, Al_2O_3, CaO contents and lower K_2O contents

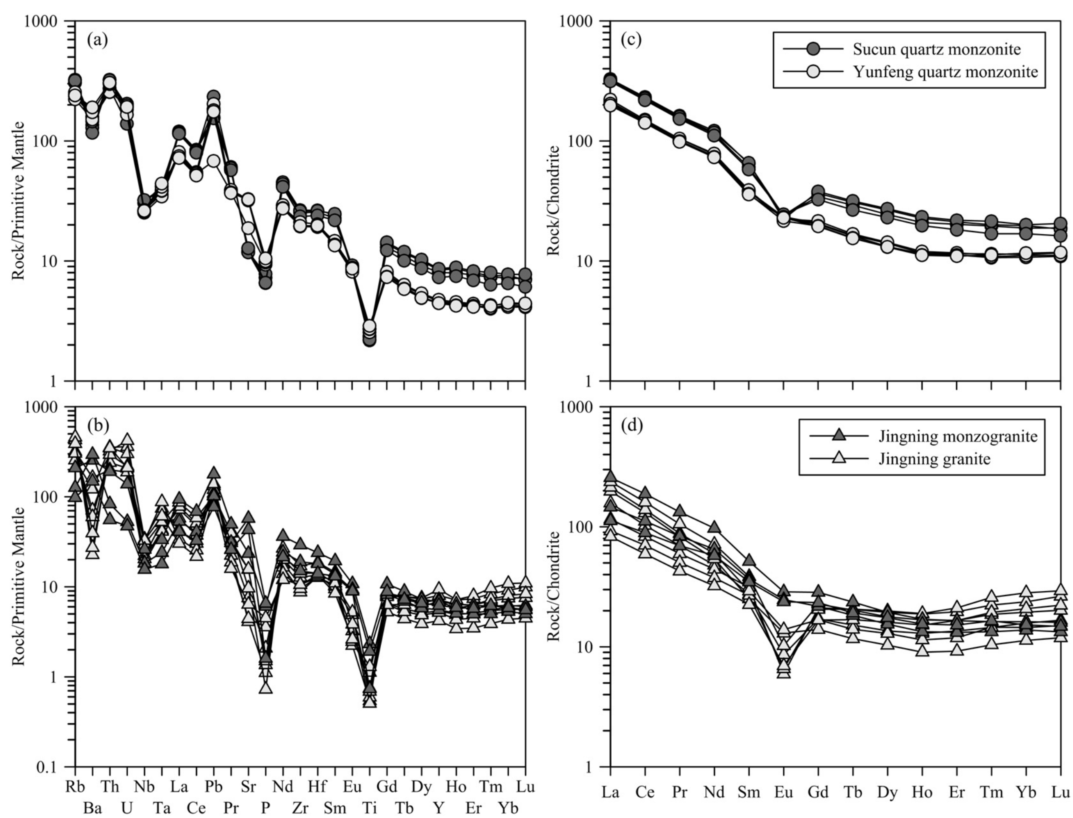

Fig. 6. (a) and (c): Primitive mantle-normalized element spider diagram; (b) and (d): Chondrite-normalized REE patterns. Normalizing values for the Primitive mantle are from McDonough and Sun (1995), and normalizing values for the Chondrite are from Sun and McDonough (1989).

Table 2
Sr-Nd isotopic data

Sample	Age (Ma)	$^{87}Rb/^{86}Sr$	$^{87}Sr/^{86}Sr$	2σ	$(^{87}Sr/^{86}Sr)_0$	$^{147}Sm/^{144}Nd$	$^{143}Nd/^{144}Nd$	2σ	$(^{143}Nd/^{144}Nd)_t$	εNd (t)	T_{DM} (Ga)	T_{2DM} (Ga)
Sucun quartz monzonite												
SC-01	136					0.104368	0.512140	0.000005	0.512047	−8.11	1.4	1.6
SC-04	136	2.2433	0.712875	0.000006	0.7085	0.105404	0.512138	0.000004	0.512044	−8.17	1.4	1.6
SC-05	136	2.3945	0.713086	0.000005	0.7085	0.110982	0.512148	0.000003	0.512049	−8.07	1.5	1.6
SC-06	136	2.1823	0.713080	0.000005	0.7089	0.103391	0.512141	0.000002	0.512049	−8.08	1.4	1.6
Yunfeng quartz monzonite												
YF-01	104	1.0947	0.710094	0.000005	0.7085	0.100275	0.512305	0.000004	0.512237	−5.21	1.1	1.3
YF-02	104	0.6747	0.709142	0.000006	0.7081	0.097782	0.512305	0.000004	0.512238	−5.19	1.1	1.3
YF-03	104	0.5975	0.709018	0.000004	0.7081	0.098459	0.512298	0.000004	0.512231	−5.32	1.1	1.3
YF-04	104	0.6776	0.709236	0.000005	0.7082	0.097749	0.512318	0.000004	0.512252	−4.93	1.1	1.3
YF-05	104	0.6449	0.709095	0.000004	0.7081	0.096927	0.512322	0.000006	0.512256	−4.85	1.1	1.3
Jingning monzogranite												
JNHX20	135	0.7784	0.720015	0.000005	0.7185	0.105025	0.511968	0.000003	0.511876	−11.51	1.7	1.9
JNHX25	135	0.1924	0.712015	0.000004	0.7116	0.111440	0.512083	0.000003	0.511985	−9.37	1.6	1.7
JNHX26	135	0.1991	0.734855	0.000005	0.7345	0.119694	0.511985	0.000005	0.511880	−11.42	1.9	1.9
Jingning granite												
JNHX01	112	3.5402	0.714661	0.000005	0.7090	0.113720	0.512136	0.000003	0.512053	−8.61	1.5	1.6
JNHX02	112	9.1470	0.723569	0.000004	0.7090	0.140099	0.512141	0.000003	0.512038	−8.89	2.1	1.6
JNHX09	112	1.4344	0.720310	0.000006	0.7180	0.092174	0.512146	0.000004	0.512078	−8.11	1.3	1.6
JNHX12	112	9.0540	0.712132	0.000006	0.6977	0.141808	0.512132	0.000004	0.512028	−9.09	2.2	1.6
JNHX13	112	1.7760	0.720855	0.000005	0.7180	0.096873	0.512141	0.000013	0.512070	−8.27	1.3	1.6
JNHX14	112	2.7453	0.723012	0.000004	0.7186	0.106336	0.512099	0.000006	0.512021	−9.23	1.5	1.7
JNHX18	112	5.3179	0.712591	0.000006	0.7041	0.138929	0.512061	0.000006	0.511959	−10.43	2.2	1.8

Notes: $^{87}Rb/^{86}Sr$ and $^{147}Sm/^{144}Nd$ ratios are calculated using Rb, Sr, Sm and Nd contents (Table 1), measured by ICP-MS; εNd(t) values are calculated using present-day $(^{147}Sm/^{144}Nd)_{CHUR} = 0.1967$ and $(^{143}Nd/^{144}Nd)_{CHUR} = 0.512638$; T_{DM} values are calculated using present-day $(^{147}Sm/^{144}Nd)_{DM} = 0.2137$ and $(^{143}Nd/^{144}Nd)_{DM} = 0.51315$; T_{2DM} is the two-stage Nd depleted-mantle model age calculated using the same assumption formulation as Keto and Jacobsen (1987).

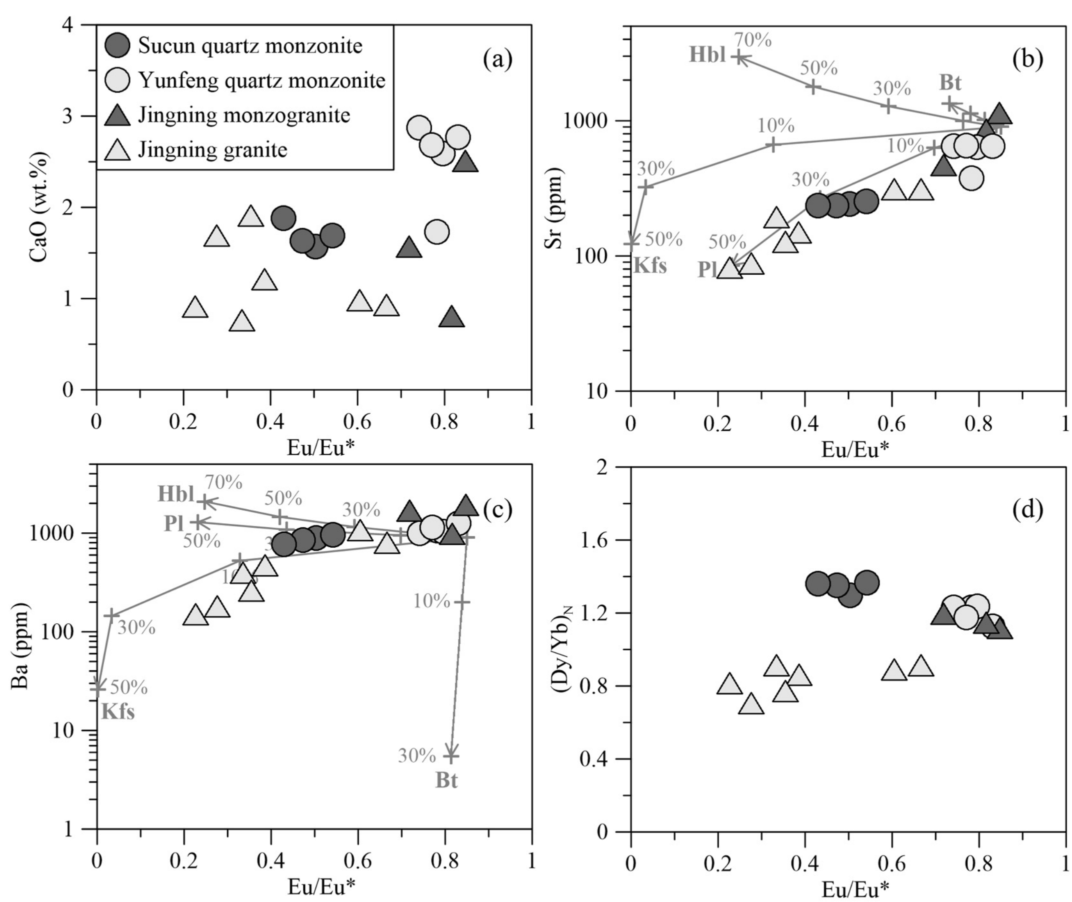

Fig. 7. (a), (b), (c), and (d) CaO, Sr, Ba, and $(Dy/Yb)_N$ versus Eu/Eu* diagrams. Applied partition coefficients for (b) and (c) are from http://earthref.org/KDD. The applied partition coefficients and their references are listed in the Appendix Table A2.

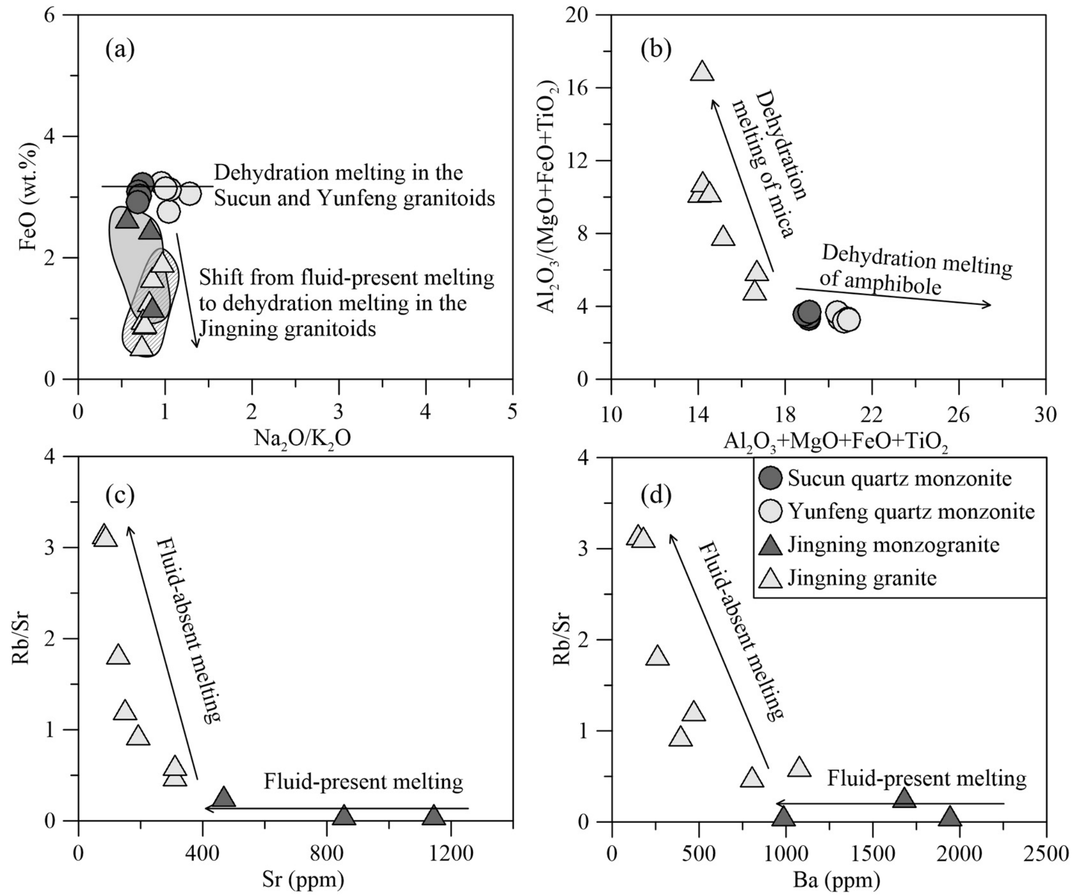

Fig. 8. (a): FeO versus Na_2O/K_2O diagram (modified after Weinberg and Hasalova, 2015); (b) $Al_2O_3/(FeO+MgO+TiO_2)$ ratios versus the total contents of $Al_2O_3 + FeO + MgO + TiO_2$ diagram (the source for the variation trend is based on Patiño Douce, 1999). (c) and (d): Rb/Sr versus Sr and Ba diagrams for the Sucun and Yunfeng quartz monzonites, and the Jingning monzogranite and granite.

than those of the Sucun quartz monzonite (Fig. 5). These geochemical compositions imply that their magma source might be probably modified by more mantle-derived melts containing high ferromagnesian, Na_2O, and CaO contents and low K_2O contents. The relatively lower REE contents of the Yunfeng quartz monzonite than those of the Sucun quartz monzonite (Fig. 6c) may also be resulted from the significant input of juvenile melts, which further support our hypothesis.

5.1.2. The Jingning monzogranite and granite

The Jingning monzogranite and granite have relatively higher SiO_2 (69.8–76.4 wt%) with metaluminous to weakly peraluminous (A/CNK = 0.99–1.09) (Table 1). Hornblende and titanite are present in the Jingning monzogranite (Fig. 2d-e). The Jingning monzogranite and granite show similar covariations in the Harker diagrams (Fig. 5). Nd isotopic compositions (Table 2) and most of the trace elements contents (Fig. 6b) of the Jingning granite are comparable to those of the Jingning monzogranite, suggesting that they have similar magma source. These features indicate that they were derived from igneous sources in the crust (Chappell, 1999; Chappell and White, 1992). However, these two intrusions clearly show a few differences in the primitive-mantle-normalized trace element patterns (Fig. 6b), suggesting that they may have different petrogenesis.

The Jingning monzogranite have higher Ba (986–1944 ppm), Sr (468–1145 ppm), and Eu (1.38–1.67 ppm with Eu/Eu* = 0.72–0.85) contents than those of the Jingning granite (Ba = 150–1078 ppm, Sr = 82–311 ppm, and Eu = 0.35–0.81 ppm with Eu/Eu* = 0.23–0.67). Both the Jingning monzogranite and granite contain constant K_2O and Na_2O contents with variable SiO_2 contents implying that these differences were not due to fractionation and crystallization of plagioclase and K-feldspar. This is further supported by irrelevances between the CaO, Sr, Ba contents, and Eu/Eu* ratios of the Jingning monzogranite and granite, although both of them exhibit fractionation and crystallization of plagioclase and K-feldspar (Fig. 7). Instead, these features are most likely to be resulted from different fluid fugacity conditions during partial melting of their magma sources. In fluid-present partial melting reactions, plagioclase and K-feldspar would firstly be out and lead to high Ba, Sr, and Eu contents in the melts (Moyen and Stevens, 2006; Weinberg and Hasalova, 2015). The high Ba, Sr, and Eu contents of the Jingning monzogranite suggest that they might be originated from fluid-present partial melting. Besides, the low Rb/Sr ratios and high Ba and Sr contents of the Jingning monzogranite are also consistent with that they were derived from water-present melting (Fig. 8c and d).

MgO and FeO concentrations in granitic melts would decrease with decreased fluid content (Conrad, Nicholls, and Wall, 1988; Patiño Douce, 1996; Weinberg and Hasalova, 2015). The decreasing FeO contents of the Jingning monzogranite and granite are consistent with a shift from fluid-present melting to dehydration melting in the Jingning granitoids (Fig. 8a). The low $Al_2O_3 + FeO + MgO + TiO_2$ contents and wide ranges of $Al_2O_3 / (FeO + MgO + TiO_2)$ ratios of the Jingning granite indicate dehydration melting of biotite (Fig. 8b). As biotite and K-feldspar have high partition coefficients of Rb and Sr, breakdown of biotite and formation of K-feldspar in the residuum would lead to high Rb/Sr ratios in the melts (Weinberg and Hasalova, 2015). Thus, the high and variable Rb/Sr ratios with relatively low Ba and Sr contents of the Jingning granite also indicate occurrence of dehydration partial melting of biotite (Fig. 8c and d). This consideration is further supported by their higher Co contents (105–145 ppm), which show high partition coefficient in biotite, than those of the Jingning monzogranite (53–92 ppm).

For the Jingning granite, the covariations of their major elements in the Harker diagram (Fig. 5) imply crystallization and fractionation. They are characterized by slightly elevated HREE patterns in the Chondrite-normalized REE pattern (Fig. 6d), indicating fractionation of hornblende which have relatively higher partition coefficients of Dy, Ho, and Er than those of Tm, Yb, and Lu. Besides, hornblende has high partition coefficients of Sc, V, Cr, Ni in granitoids. The Jingning granite exhibit lower Sc (1.69–3.92 ppm), V (5.30–17.80 ppm), Cr (0.52–0.90 ppm), Ni (1.87–2.66 ppm) contents than those of the Jingning monzogranite (Sc = 7.27–20.50 ppm, V = 25–182 ppm, Cr = 0.63–30.80 ppm, Ni = 1.88–12.20 ppm), which is consistent with fractionation of hornblende.

The Jingning monzogranite exhibit $\varepsilon_{Nd}(t)$ values of −11.51 to −9.37 with T_{2DM} of 1.7–1.9 Ga (Table 2), indicating they were derived from the mature lower crust of our study area. Two-stage crustal model ages (1.7–1.9 Ga) of the Jingning monzogranite are comparable with the Paleoproterozoic Badu Group, implying they were originated from the Badu Group. The Jingning granite have slightly higher $\varepsilon_{Nd}(t)$ values of −10.43 to −8.11 with T_{2DM} of 1.6–1.8 Ga (Table 2), suggesting that the Badu Group may also be the dominated magma source for the Jingning granite and their magma sources have insignificant input of juvenile materials.

5.2. Geodynamical implication

The North China Craton, as one of the oldest craton in East Asia, stand stable from Paleoproterozoic to Paleozoic with a cold and thick lithosphere and transformed to a hot and thin lithosphere during Meosozoic to Cenozoic (Fan et al., 2000; Griffin, Andi, O'Reilly, and Ryan, 1998; Menzies, 1993). Fluids/melts derived from three Phanerozoic ocean slab subductions (the Tethyan, Paleo-Asian, and Paleo-Pacific plate, respectively) were proposed to lead to refertilization of the originally refractory lithospheric mantle underlying the North China Craton through fluid/melt-rock interaction, which would lower the viscosity, weaken the rheology, and increase the density of the SCLM significantly (Meng and Zhang, 1999; Menzies, Xu, Zhang, and Fan, 2007; Wu et al., 2005; Xiao, Windley, Hao, and Zhai, 2003). Besides, extensive partial melting during Phanerozoic might form eclogitic lower crust of the North China craton (Wu et al., 2005; Wu, Jahn, Wilde, and Sun, 2000). The resultant density instability of the North China Craton lithosphere would lead to detachment, foundering and lithospheric thinning (Anderson, 2005; Gao et al., 2004). Nevertheless, the peak timing of lithospheric destruction in North China Craton is widely accepted to be Early Cretaceous (130–120 Ma) (Dai, Zheng, and Zhao, 2016; Menzies et al., 2007; Wu et al., 2005; Zhu et al., 2012). Furthermore, lithospheric destruction occurred concentratedly in the east side of the North China Craton and became insignificant westward (Sun, Liu, Zhang, Li, and Qi, 2017; Zhai, Fan, Zhang, Sui, and Shao, 2007; Zhang et al., 2004). These features imply that the Paleo-Pacific plate subduction during Late Mesozoic play the dominated role in the lithospheric destruction of the North China Craton. However, the detailed timing, characteristics, and processes remain unclear, because the influences of the Paleo-Pacific plate subduction were easily modified by the subsequent lithospheric destruction in this area.

Parts of the South China Block have been considered to be destroyed according to a few lines of evidences, including P-wave tomographic results (Jiang, Zhang, Lu, Shi, and Xu, 2013), lithospheric mantle xenoliths (Liu et al., 2012; Lu et al., 2013; Xu et al., 2000; Zheng et al., 2015), magma source variations of mantle-derived mafic rocks (X. Li et al., 2014; Yan, Chen, and Xu, 2008), and heat flow values (Li et al., 2015 and references therein). However, both of refractory and fertile lithospheric mantle xenoliths were commonly found in these areas (Liu et al., 2012; Lu et al., 2013; Xu et al., 2000; Zheng et al., 2015), implying that the lithospheric mantle is strongly heterogeneous. Thus, the lithospheric modification in South China Block may be generally weaker than the North China Craton destruction, and geological records of the modification processes probably were better preserved in South China Block.

Extensive Late Mesozoic granitoids found in South China (Chen et al., 2000; Li and Li, 2007; Zhou and Li, 2000) may record the secular evolution

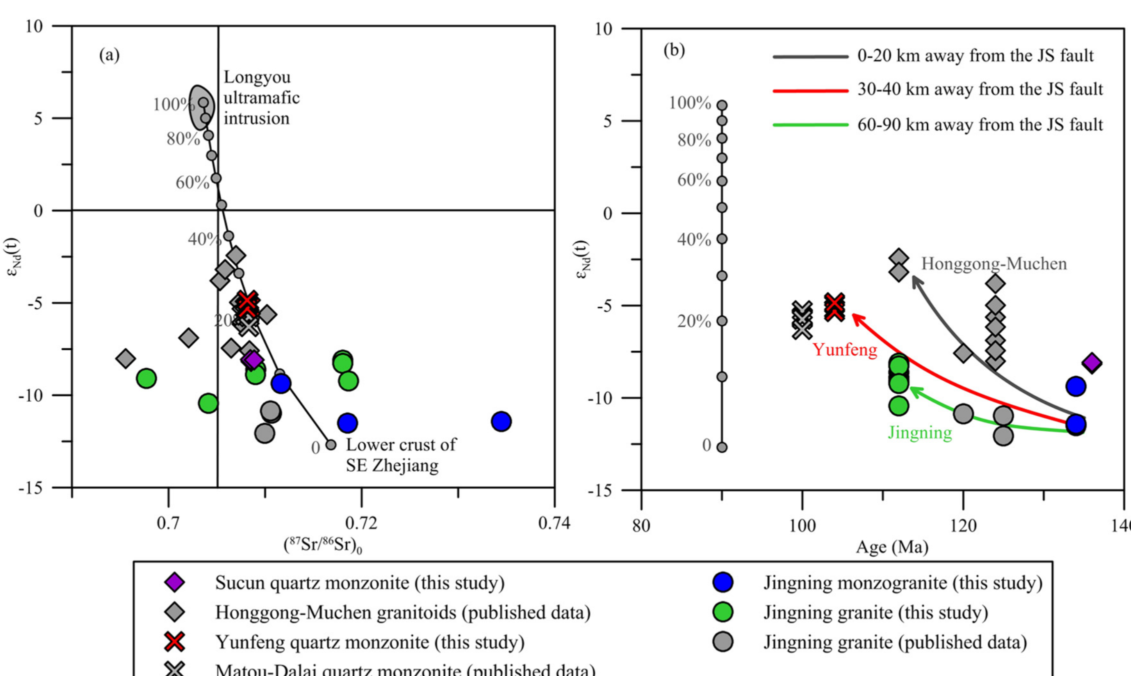

Fig. 9. (a): $\varepsilon_{Nd}(t)$ versus $(^{87}Sr/^{86}Sr)_0$ diagram for the Sucun and Yunfeng quartz monzonites, and the Jingning monzogranite and granite. The published data for Honggong–Muchen granitoids, Yunfeng (Matou–Dalai) quartz monzonites, and Jingning granite are from Chen et al. (1999), Wang et al. (1997), Shen et al. (1999), Liu et al. (2012b), and Liu et al. (2014b). (b): The estimated amounts of mantle-derived materials for their magma sources based on Nd isotopic binary mixing model. The Honggong–Muchen (grey line), Yunfeng (red line), and Jingning (green line) granitoids are located at 0–20 km, 30–40 km, and 60–90 km away from the JS fault, respectively. The distinct gradients of these lines show different contributions of mantle-derived materials in their magma sources.

of lower crust in this area, which could provide an opportunity for understanding the detailed influences of the coeval Paleo-Pacific plate subduction. As pointed out above, published Nd isotopic data exhibit an obvious shift from the Triassic granites containing relatively homogeneous compositions of −11 to −15 with T_{2DM} of 2.0 to 2.2 Ga (Li et al., 2012; Mao et al., 2013; Sun et al., 2011; Xu et al., 2013; Zhao et al., 2013), to the Cretaceous granitoids having less enriched and more heterogeneous compositions of −2 to −13 with T_{2DM} of 1.1 to 1.9 Ga (Chen, Guo, Tang, and Zhou, 1999; Liu et al., 2012b, 2014b; Shen et al., 1999; Wang, Zhao, Bao, and Li, 1997) in Zhejiang, NE South China Block. These features indicate the magma sources for the Cretaceous granitoids have significant input of mantle-derived juvenile materials during Late Mesozoic.

The petrogenesis discussion above shows that the magma source of the Sucun quartz monzonite was slightly modified by the mantle-derived juvenile materials and the magma source for the Yunfeng quartz monzonite may be probably modified by more mantle-derived melts. Besides, the Jingning granite also has slightly higher Nd isotopic compositions than those of the Jingning monzogranite (Table 2). The Nd isotopic composition variations of the Early Cretaceous granitoids in this study are consistent with input of mantle-derived juvenile materials. For further assessing the influence of the mantle-derived melts, we take the Early Cretaceous Longyou ultramafic intrusions as the end member of upwelling asthenosphere (Qi et al., 2016), mixed with the lower crust replaced by the Early Cretaceous granitoids with clearly enriched Nd isotopic compositions (Fig. 9). Although the Badu Group was considered to be the dominant magma source for these Cretaceous granitoids in the studied area, it is not a homogeneous unit (Yu et al., 2012) and may be modified during the Mesozoic multistage magmatism (C.-H. Chen et al., 2016; Chen et al., 2000; Liu et al., 2016; P. Li et al., 2013; Qiu et al., 2004; Wong et al., 2011; Z. Li et al., 2013; Zhao et al., 2016). Published Sm–Nd isotopic data of the Badu Group show that the mafic amphibolites were originated from an extremely depleted mantle source during the Paleoproterozoic (~1.8 Ga) (Li et al., 2000), and the granitoids were derived from reworking of the Archean (2.6–2.9 Ga) continental material (Yu et al., 2012; Zhao et al., 2014). It is difficult to identify the contributions of these components on the magma geochemistry of the Cretaceous granitoids in the studied area. Thus, here we take the Early Cretaceous granitoids with the enriched Nd isotopic composition (Sr = 200 ppm, Nd = 22.56 ppm, $^{87}Sr/^{86}Sr$ = 0.71682, $^{143}Nd/^{144}Nd$ = 0.5119) as one end-member in the simple binary mixing model (Fig. 9a). A few granitoid samples deviating from the mixing curve are attributed to their variable Sr isotopic compositions, which could be resulted from their low Sr compositions and high $^{87}Rb/^{86}Sr$ ratios (Table 2) as well as Sr isotopic modification of their magma source during granulite-facies metamorphism related to collisional orogeny at 1.89–1.88 Ga and 252–234 Ma (Yu et al., 2012). We hence tend to obtain a rough estimate of juvenile material contribution based on the Nd isotopic compositions (Fig. 9b). Our modeling shows a notably decreasing content of juvenile material input away from JS fault during Early Cretaceous, 30% for 0–20 km, 20% for 30–40 km, and 10% for 60–90 km, respectively (Fig. 9b).

Cretaceous volcanic basins are widely distributed in Zhejiang, which belong to the northeast part of the huge 'South China Extensional Basin and Igneous Province' (Zhou, Sun, Shen, Shu, and Niu, 2006). Most basins from northwest Zhejiang are NE-trending, whereas both of NE-trending and NW-trending for the southeast Zhejiang basins. Widespread extension and asthenosphere mantle upwelling, which were caused by subduction of the Paleo-Pacific slab, likewise promoted destruction of the back-arc lithosphere (Jiang et al., 2015; Jiang, Zhao, Zhou, Liao, and Jin, 2011; Sun et al., 2011; Wong et al., 2009; Yang et al., 2012). Here we provide a reformative geodynamic hypothesis as below based on the tectono-magmatic evolution in Zhejiang, NE South China Block.

The northwest Zhejiang basins are dominantly composed of Early Cretaceous (~140–120 Ma) volcanic rocks with coeval detrital rocks (BGMRZP, 1989; J. Li et al., 2014; Liu, Xu, and Xia, 2014a). The volcaniclastic contents clearly decrease upward in these Early Cretaceous strata (BGMRZP, 1989). Contemporaneous (~140–120 Ma) volcanic and detrital rocks are widely distributing in southeast Zhejiang (BGMRZP, 1989; Liu et al., 2012a), which shows probably more intense volcanism compared to the northwest Zhejiang volcanism. These features show that the Early Cretaceous volcanism in northwest Zhejiang basins might be formed in back-arc setting (Fig. 10a). Minor asthenosphere-derived melts, represented by the Longyou ultramafic intrusions (Qi et al., 2016 and our unpublished data), might rise through the JS fault in an extensional setting and modify the lithosphere nearby (Fig. 10a). The volcanic and detrital rocks in the southeast Zhejiang basins are relatively younger (~110–88 Ma) (BGMRZP, 1989; Liu et al., 2012a). Contemporaneous volcanic rocks nearly ceased in northwest Zhejiang and are locally found in Jin-Qu basin (Yu et al., 2004 and our unpublished data), subparallel to the JS fault (Fig. 1c). These geological features imply that the magmatic front progressively eastward migrated and the magmatic activities became weakening in interior Zhejiang (Fig. 10b). Besides, the back-arc extension represented by the Cretaceous basins in Zhejiang also eastward migrated (Fig. 10b). The migration of the Paleo-Pacific plate subduction, represented by the migration of the magmatic front and the Cretaceous basins, caused intense upwelling of the hot asthenosphere in interior Zhejiang during Early Cretaceous (~120–100 Ma) which can be found along the JS fault (Yu et al., 2004 and our unpublished data). The asthenosphere upwelling may result in obvious mantle-derived melts intruded into the lower crust, especially near the JS fault (Fig. 10b). To sum up, we propose that roll-back and retreat of the Paleo-Pacific plate subduction might cause extensive asthenosphere mantle upwelling, and the mantle-derived melts tend to

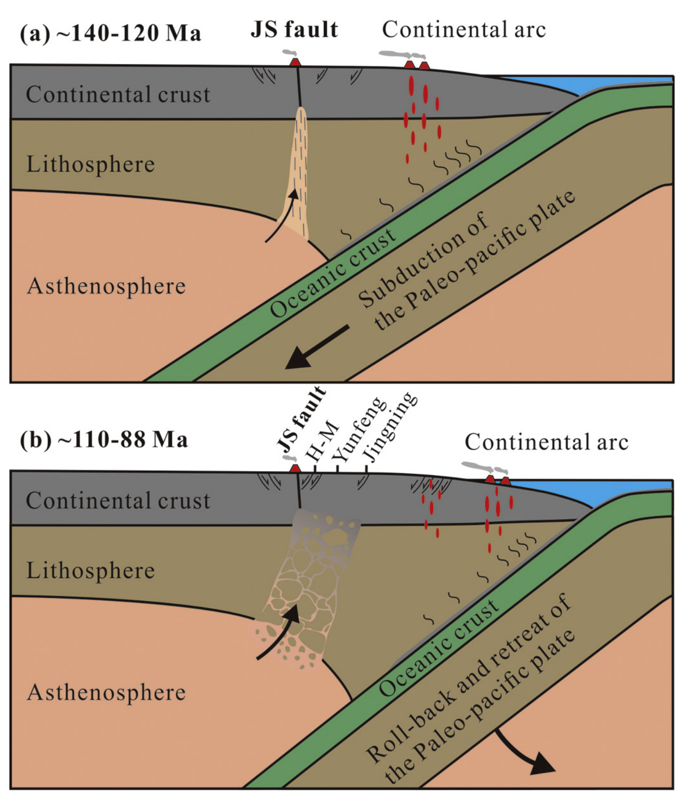

Fig. 10. Schematic tectonic model for the source evolution of the Cretaceous Sucun and Yunfeng quartz monzonites, and the Jingning monzogranite and granite. Minor asthenosphere-derived melts rose through the JS fault during ~140–120 Ma in a back-arc extensional setting (a). Then, the roll-back and retreat of the Paleo-Pacific plate subduction during ~110–88 Ma caused more intense back-arc extensions and upwelling of the hot asthenosphere in the coastal area during Early Cretaceous (b). The mantle-derived melts tended to rise through the JS fault and preferentially modify the lithosphere nearby these faults. H–M: Honggong–Muchen.

rise through the regional main fault zones (e.g. the JS fault) and preferentially modify the lithosphere nearby these faults. These processes may be common in lithosphere destruction and refertilization in East China and adjacent areas.

6. Conclusions

The Early Cretaceous Sucun (136 Ma), Yunfeng (104 Ma), and Jingning (135 and 112 Ma) intrusions from southwest Zhejiang, NE South China Block, are presented to trace their petrogenesis and implications for lithosphere evolution. All these intrusions are metaluminous to weakly peraluminous and high-K calc-alkaline series. The Yunfeng quartz monzonite clearly have lower K_2O and total REE contents, and higher CaO, Na_2O, Al_2O_3, P_2O_5, MgO, and TiO_2 contents, and relatively less enriched Sr–Nd isotopic compositions than those of the Sucun quartz monzonite. These quartz monzonites were derived from amphibole-dehydration partial melting of lower crust. The Jingning monzogranite exhibits similar major elements covariations and Nd isotopic compositions, but higher Ba, Sr, and Eu contents and lower Rb, Th, and U contents than those of the Jingning granite. The geochemical features imply that the Jingning monzogranite and granite were the fluid-present and fluid-absent anatexis products of the same crustal source, respectively. Whole-rock Sr–Nd isotopic data imply that the estimated amounts of mantle-derived melts inputting the mature crust show southeastward decreasing trend away from the Jiangshan–Shaoxing fault. The roll-back and retreat of the Paleo-Pacific plate subduction might cause extensive asthenosphere mantle upwelling, which tend to rise through the regional main fault zones and preferentially modified the lithosphere nearby these faults during Early Cretaceous (135–104 Ma). These processes may play the dominated role in lithosphere destruction and refertilization in East China and surroundings.

Acknowledgement

This research is supported by the National Natural Science Foundation of China (Grant No. 41603026) and Department of Land and Resources of Zhejiang Province of China (Grant No. 201211013 and 2014006). The authors thank Z.C. Hu, K.Q. Zong, H.H. Chen, and L. Zhou of State Key Laboratory of Geological Process and Mineral Resources, China University of Geosciences, Wuhan for their assistance in LA–ICPMS zircon U–Pb dating and geochemical analyses. Two anonymous reviewers are thanked for their constructive comments and suggestions that helped to improve this manuscript.

Appendix

Appendix Table A1
LA-ICPMS zircon U-Pb analyses.

Spot no.	Th (ppm)	U (ppm)	Th/U	$^{207}Pb/^{206}Pb$	±1σ	$^{207}Pb/^{235}U$	±1σ	$^{206}Pb/^{238}U$	±1σ	$^{207}Pb/^{235}U$ age (Ma)	±1σ	$^{206}Pb/^{238}U$ age (Ma)	±1σ
Sucun quartz monzonite													
SC-05-01	336	448	0.75	0.0491	0.0030	0.1396	0.0084	0.0212	0.0004	132.7	7.5	135.5	2.3
SC-05-02	302	384	0.79	0.0517	0.0031	0.1533	0.0089	0.0217	0.0003	144.9	7.9	138.1	1.9
SC-05-03	156	194	0.81	0.1250	0.0088	0.4212	0.0314	0.0238	0.0006	356.9	22.4	151.6	3.6
SC-05-04	235	230	1.02	0.0493	0.0035	0.1463	0.0098	0.0220	0.0004	138.7	8.6	140.4	2.6
SC-05-05	623	814	0.77	0.0482	0.0021	0.1349	0.0056	0.0203	0.0003	128.5	5.0	129.7	1.6
SC-05-06	172	201	0.86	0.0583	0.0042	0.1686	0.0118	0.0213	0.0004	158.2	10.2	136.1	2.4
SC-05-07	154	151	1.02	0.0980	0.0100	0.3217	0.0426	0.0217	0.0006	283.2	32.7	138.2	3.8
SC-05-08	408	563	0.73	0.0463	0.0024	0.1366	0.0070	0.0213	0.0002	130.0	6.3	136.0	1.5
SC-05-09	347	519	0.67	0.0520	0.0029	0.1523	0.0084	0.0214	0.0003	143.9	7.4	136.5	1.8
SC-05-10	491	679	0.72	0.0509	0.0023	0.1469	0.0067	0.0209	0.0003	139.2	6.0	133.4	1.7
SC-05-11	596	992	0.60	0.0476	0.0020	0.1390	0.0059	0.0211	0.0002	132.2	5.2	134.9	1.4
SC-05-12	1168	1265	0.92	0.0481	0.0017	0.1435	0.0049	0.0217	0.0002	136.2	4.3	138.2	1.2
SC-05-13	349	408	0.85	0.0523	0.0030	0.1513	0.0084	0.0213	0.0003	143.0	7.5	135.8	2.0
SC-05-14	311	378	0.82	0.0529	0.0033	0.1546	0.0092	0.0216	0.0003	146.0	8.1	137.8	2.1
SC-05-15	384	670	0.57	0.0509	0.0025	0.1487	0.0070	0.0213	0.0002	140.8	6.2	135.9	1.5
SC-05-16	628	1064	0.59	0.0579	0.0023	0.1747	0.0071	0.0218	0.0003	163.5	6.1	138.9	2.0
SC-05-17	371	327	1.14	0.0508	0.0032	0.1493	0.0094	0.0214	0.0003	141.3	8.3	136.8	1.9
SC-05-18	548	784	0.70	0.0478	0.0024	0.1404	0.0071	0.0214	0.0003	133.4	6.3	136.6	1.7
SC-05-19	504	707	0.71	0.0490	0.0023	0.1441	0.0066	0.0213	0.0003	136.7	5.9	136.2	1.6
SC-05-20	216	259	0.83	0.0530	0.0037	0.1490	0.0096	0.0213	0.0004	141.0	8.5	135.6	2.3
Yunfeng quartz monzonite													
YF-02-01	214	221	0.97	0.0711	0.0059	0.1661	0.0117	0.0178	0.0003	156.1	10.2	113.6	2.1
YF-02-02	211	180	1.17	0.0596	0.0048	0.1297	0.0099	0.0163	0.0003	123.8	8.9	104.0	2.1
YF-02-03	264	175	1.51	0.0681	0.0055	0.1502	0.0109	0.0164	0.0003	142.1	9.6	104.8	2.1
YF-02-04	279	222	1.26	0.0693	0.0049	0.1535	0.0108	0.0163	0.0003	145.0	9.5	104.4	2.0
YF-02-05	266	231	1.15	0.0650	0.0054	0.1447	0.0115	0.0167	0.0004	137.2	10.2	106.5	2.4
YF-02-06	71	595	0.12	0.1134	0.0026	3.9622	0.0925	0.2508	0.0023	1626.5	18.9	1442.8	11.9
YF-02-07	246	264	0.93	0.0638	0.0055	0.1374	0.0104	0.0158	0.0003	130.7	9.3	101.3	1.8
YF-02-08	226	203	1.11	0.0665	0.0046	0.1479	0.0097	0.0164	0.0004	140.1	8.6	105.1	2.4
YF-02-09	99	301	0.33	0.1128	0.0023	5.1742	0.1010	0.3293	0.0027	1848.4	16.6	1834.9	13.2
YF-02-10	230	153	1.51	0.0984	0.0092	0.2291	0.0210	0.0167	0.0004	209.5	17.3	106.9	2.4
YF-02-11	286	240	1.20	0.0719	0.0055	0.1560	0.0114	0.0158	0.0003	147.2	10.0	100.9	1.9
YF-02-12	274	238	1.15	0.0598	0.0035	0.1285	0.0071	0.0156	0.0003	122.7	6.4	100.0	1.7
YF-02-13	693	345	2.01	0.0933	0.0074	0.2180	0.0211	0.0158	0.0003	200.3	17.6	101.3	1.9
YF-02-14	242	213	1.13	0.0691	0.0049	0.1576	0.0099	0.0171	0.0003	148.6	8.6	109.3	2.0
YF-02-15	251	175	1.43	0.0667	0.0062	0.1378	0.0105	0.0159	0.0004	131.1	9.4	101.7	2.5
YF-02-16	196	139	1.41	0.1028	0.0081	0.2244	0.0169	0.0166	0.0004	205.6	14.0	106.2	2.7
YF-02-17	635	280	2.27	0.0653	0.0046	0.1461	0.0093	0.0168	0.0003	138.5	8.2	107.4	2.2
YF-02-18	277	235	1.18	0.0655	0.0047	0.1424	0.0089	0.0162	0.0003	135.1	7.9	103.7	2.0
YF-02-19	411	280	1.47	0.0647	0.0044	0.1317	0.0084	0.0154	0.0003	125.7	7.6	98.6	1.9

(continued on next page)

Appendix Table A1 (*continued*)

Spot no.	Th (ppm)	U (ppm)	Th/U	^{207}Pb/^{206}Pb	±1σ	^{207}Pb/^{235}U	±1σ	^{206}Pb/^{238}U	±1σ	^{207}Pb/^{235}U age (Ma)	±1σ	^{206}Pb/^{238}U age (Ma)	±1σ
YF-02-20	614	301	2.04	0.0509	0.0038	0.1145	0.0074	0.0167	0.0003	110.1	6.8	106.8	1.8
Jingning monzogranite													
JNHX-26-01	262	214	1.22	0.0755	0.0056	0.2458	0.0193	0.0235	0.0005	223.2	15.7	149.5	2.8
JNHX-26-02	204	199	1.02	0.0669	0.0047	0.2044	0.0139	0.0226	0.0005	188.8	11.7	144.3	2.9
JNHX-26-03	799	894	0.89	0.0496	0.0022	0.1432	0.0062	0.0208	0.0002	135.9	5.5	132.8	1.4
JNHX-26-04	693	843	0.82	0.0498	0.0019	0.1421	0.0056	0.0206	0.0002	134.9	5.0	131.2	1.5
JNHX-26-05	507	418	1.21	0.0571	0.0031	0.1615	0.0083	0.0206	0.0003	152.0	7.3	131.3	1.8
JNHX-26-07	238	250	0.95	0.0620	0.0039	0.1918	0.0122	0.0224	0.0004	178.2	10.4	142.6	2.5
JNHX-26-08	2361	579	4.08	0.0536	0.0048	0.1528	0.0139	0.0204	0.0003	144.3	12.3	129.9	1.7
JNHX-26-09	296	290	1.02	0.0741	0.0050	0.2419	0.0169	0.0233	0.0004	219.9	13.8	148.5	2.7
JNHX-26-10	100	84	1.18	0.1066	0.0097	0.2885	0.0243	0.0227	0.0007	257.4	19.1	144.7	4.5
JNHX-26-11	76	94	0.81	0.1118	0.0092	0.3189	0.0243	0.0220	0.0006	281.1	18.7	140.1	3.7
JNHX-26-12	1069	2445	0.44	0.0524	0.0016	0.1511	0.0046	0.0208	0.0003	142.9	4.1	132.9	1.6
JNHX-26-13	545	653	0.83	0.0497	0.0022	0.1427	0.0062	0.0207	0.0003	135.5	5.5	132.4	1.7
JNHX-26-14	326	305	1.07	0.0747	0.0044	0.2362	0.0149	0.0225	0.0004	215.3	12.2	143.6	2.6
JNHX-26-15	105	84	1.25	0.1058	0.0090	0.2794	0.0185	0.0208	0.0006	250.2	14.7	132.6	3.6
JNHX-26-16	358	295	1.21	0.0716	0.0048	0.2136	0.0141	0.0221	0.0004	196.6	11.8	140.7	2.6
JNHX-26-17	248	220	1.13	0.0610	0.0038	0.1778	0.0114	0.0211	0.0004	166.2	9.8	134.8	2.3
JNHX-26-18	354	464	0.76	0.0513	0.0031	0.1429	0.0084	0.0203	0.0003	135.7	7.4	129.9	1.8
JNHX-26-19	374	380	0.98	0.0605	0.0035	0.1658	0.0093	0.0203	0.0003	155.8	8.1	129.7	2.2
JNHX-26-20	35	32	1.08	0.2241	0.0210	0.5606	0.0359	0.0208	0.0009	451.9	23.4	132.9	5.8
Jingning granite													
JNHX-09-01	1170	659	1.78	0.0536	0.0033	0.1219	0.0064	0.0166	0.0003	116.8	5.8	106.3	1.6
JNHX-09-02	478	948	0.50	0.0469	0.0019	0.1124	0.0047	0.0175	0.0003	108.2	4.3	111.9	1.7
JNHX-09-03	296	776	0.38	0.0514	0.0023	0.1556	0.0064	0.0221	0.0003	146.9	5.7	140.9	1.8
JNHX-09-04	131	186	0.71	0.0622	0.0046	0.1465	0.0101	0.0175	0.0004	138.8	9.0	111.8	2.3
JNHX-09-05	740	1476	0.50	0.0491	0.0020	0.1153	0.0053	0.0166	0.0004	110.8	4.9	106.0	2.4
JNHX-09-06	286	518	0.55	0.0529	0.0026	0.1333	0.0062	0.0180	0.0002	127.0	5.6	115.0	1.3
JNHX-09-07	191	335	0.57	0.0535	0.0038	0.1314	0.0092	0.0181	0.0003	125.4	8.2	115.7	1.8
JNHX-09-08	633	1807	0.35	0.0571	0.0021	0.1159	0.0044	0.0148	0.0003	111.3	4.0	94.7	2.0
JNHX-09-09	325	645	0.50	0.0496	0.0023	0.1219	0.0053	0.0180	0.0002	116.8	4.8	114.8	1.3
JNHX-09-10	122	224	0.55	0.0529	0.0039	0.1634	0.0120	0.0227	0.0004	153.7	10.5	144.6	2.7
JNHX-09-11	158	253	0.62	0.0499	0.0030	0.1209	0.0070	0.0179	0.0004	115.8	6.3	114.6	2.2
JNHX-09-16	328	521	0.63	0.0605	0.0033	0.1432	0.0077	0.0171	0.0002	135.9	6.9	109.6	1.6
JNHX-09-17	255	240	1.06	0.0609	0.0042	0.1404	0.0092	0.0175	0.0003	133.4	8.2	111.5	2.2
JNHX-09-18	471	930	0.51	0.0493	0.0024	0.1171	0.0054	0.0173	0.0002	112.5	4.9	110.3	1.2
JNHX-09-19	418	700	0.60	0.0482	0.0030	0.1183	0.0068	0.0180	0.0002	113.5	6.2	115.1	1.4
JNHX-09-20	171	265	0.64	0.0587	0.0036	0.1408	0.0087	0.0180	0.0004	133.8	7.8	115.0	2.3

Appendix Table A2
The applied partition coefficients and their references

	Hbl	Bi	Kfs	Pl
Ba	0.3	15.3	6.12	0.48
Sr	0.01	0.672	3.87	4.4
Sm	2.3	0.392	0.026	0.12
Eu	3.2	0.501	9.06	2
Gd	2	0.353	0.011	0.129

References

Bacon, C.R. and Druitt, T.H. (1988). Compositional Evolution of the Zoned Calcalkaline Magma Chamber of Mount-Mazama, Crater Lake, Oregon. Contributions to Mineralogy and Petrology 98(2): 224-256.

Philpotts, J.A. and Schnetzler, C.C. (1970). Phenocryst-matrix partition coefficients for K, Rb, Sr and Ba, with applications to anorthosite and basalt genesis. Geochimica et Cosmochimica Acta 34(3): 307-322. doi: 10.1016/0016-7037(70)90108-0.

Schnetzler, C.C. and Philpotts, J.A. (1970). Partition coefficients of rare-earth elements between igneous matrix material and rock-forming mineral phenocrysts; II. Geochimica et Cosmochimica Acta 34(3): 331-340. doi: 10.1016/0016-7037(70)90110-9.

Leeman, W.P. and Phelps, D.W. (1981). Partitioning of rare earths and other trace elements between sanidine and coexisting volcanic glass. Journal of Geophysical Research 86: doi: 10.1029/JB080i011p10193. issn: 0148-0227.

Nagasawa, H. and Schnetzler, C.C. (1971). Partitioning of rare Earth, alkali, and alkaline Earth elements between phenocrysts and acidic igneous magmas. Geochimica et Cosmochimica Acta 35: 953-968. doi: 10.1016/0016-7037(71)90008-1.

References

Anderson, D.L., 2005. Large igneous provinces, delamination, and fertile mantle. Elements 1, 271–275.

BGMRZP, 1989. Reginal Geology of Zhejiang Province. Geological Publishing House, Beijing, pp. 1–688 (Bureau of Geology and Mineral Resources of Zhejiang Province).

Chappell, B.W., 1999. Aluminium saturation in I- and S-type granites and the characterization of fractionated haplogranites. Lithos 46, 535–551.

Chappell, B.W., White, A.J.R., 1992. I- and S-type granites in the Lachlan Fold Belt. Transactions of the Royal Society of Edinburgh: Earth Sciences 83, 1–26.

Chen, J.F., Guo, X.S., Tang, J.F., Zhou, T.X., 1999. Nd isotopic model ages: implications of the growth of the continental crust of southeastern China. Journal of Nanjing University (Natural Sciences) 35, 649–658.

Chen, C., Lin, W., Lu, H., Lee, C., Tien, J., Lai, Y., 2000. Cretaceous fractionated I-type granitoids and metaluminous A-type granites in SE China: the Late Yanshanian post-orogenic magmatism. Transactions of the Royal Society of Edinburgh: Earth Sciences 350, 195–205.

Chen, C.-H., Lee, C.-Y., Shinjo, R., 2016a. The epilog of the western paleo-Pacific subduction: inferred from spatial and temporal variations and geochemistry of the Late Cretaceous to Early Cenozoic silicic magmatism in coastal South China. Journal of Asian Earth Sciences 115, 520–546.

Chen, C., Liu, Y., Foley, S.F., Ducea, M.N., He, D., Hu, Z., Chen, W., Zong, K., 2016b. Paleo-Asian oceanic slab under the North China craton revealed by carbonatites derived from subducted limestones. Geology 44, 1039–1042.
Conrad, W.K., Nicholls, I.A., Wall, V.J., 1988. Water-saturated and -undersaturated melting of metaluminous and peraluminous crustal compositions at 10 kb: evidence for the origin of silicic magmas in the Taupo Volcanic Zone, New Zealand, and other occurrences. Journal of Petrology 29, 765–803.
Corfu, F., Hanchar, J.M., Hoskin, P.W.O., Kinny, P.D., 2003. Atlas of zircon textures. Reviews in Mineralogy and Geochemistry 53, 469–500.
Dai, L., Zheng, Y., Zhao, Z., 2016. Termination time of peak decratonization in North China: geochemical evidence from mafic igneous rocks. Lithos 240–243, 327–336.
Fan, W.M., Zhang, H., Baker, J.A., Jarvis, K.E., Mason, P.R.D., Menzies, M.A., 2000. On and off the North China Craton: where is the Archaean Keel? Journal of Petrology 41, 933–950.
Gao, S., Rudnick, R.L., Carlson, R.W., Mcdonough, W.F., Liu, Y., 2002. Re–Os evidence for replacement of ancient mantle lithosphere beneath the North China craton. Earth and Planetary Science Letters 198, 307–322.
Gao, S., Rudnick, R.L., Yuan, H.L., Liu, X.M., Liu, Y.S., Xu, W.L., Ling, W.L., Ayers, J., Wang, X.C., Wang, Q.H., 2004. Recycling lower continental crust in the North China craton. Nature 432, 892–897.
Griffin, W.L., Andi, Z., O'Reilly, S.Y., Ryan, C.G., 1998. Phanerozoic evolution of the lithosphere beneath the Sino-Korean Craton. Mantle Dynamics and Plate Interactions in East Asia. American Geophysical Union, pp. 107–126.
Ho, K., Chen, J., Lo, C., Zhao, H., 2003. ^{40}Ar–^{39}Ar dating and geochemical characteristics of late Cenozoic basaltic rocks from the Zhejiang-Fujian region, SE China: eruption ages, magma evolution and petrogenesis. Chemical Geology 197, 287–318.
Hong, L.B., Zhang, Y.H., Xu, Y.-G., Ren, Z.-Y., Yan, W., Ma, Q., Ma, L., Xie, W., 2017. Hydrous orthopyroxene-rich pyroxenite source of the Xinkailing high magnesium andesites, Western Liaoning: implications for the subduction-modified lithospheric mantle and the destruction mechanism of the North China Craton. Lithos 282–283, 10–22.
Hu, X., Xu, J., Tong, C., Chen, C., 1991. The Precambrian Geology of Southwestern Zhejiang Province. Geological Publishing House, Beijing, pp. 1–278.
Huang, X., Su, B., Zhou, M.-F., Gao, J.-F., Qi, L., 2017. Cenozoic basalts in SE China: chalcophile element geochemistry, sulfide saturation history, and source heterogeneity. Lithos 282–283, 215–227.
Jiang, Y.-H., Zhao, P., Zhou, Q., Liao, S.-Y., Jin, G.-D., 2011. Petrogenesis and tectonic implications of Early Cretaceous S- and A-type granites in the northwest of the Gan-Hang rift, SE China. Lithos 121, 55–73.
Jiang, G., Zhang, G., Lu, Q., Shi, D., Xu, Y., 2013. 3-D velocity model beneath the Middle-Lower Yangtze River and its implication to the deep geodynamics. Tectonophysics 606, 36–47.
Jiang, Y.-H., Wang, G.-C., Liu, Z., Ni, C.-Y., Qing, L., Zhang, Q., 2015. Repeated slab advance–retreat of the Palaeo-Pacific plate underneath SE China. International Geology Review 57, 472–491.
Keto, L.S., Jacobsen, S.B., 1987. Nd and Sr isotopic variations of Early Paleozoic oceans. Earth and Planetary Science Letters 84, 27–41.
Lapierre, H., Jahn, B.M., Charvet, J., Yu, Y.W., 1997. Mesozoic felsic arc magmatism and continental olivine tholeiites in Zhejiang province and their relationship with the tectonic activity in southeastern China. Tectonophysics 274, 321–338.
Li, X.-H., 1997. Timing of Cathaysia block formation: constraints from SHRIMP U–Pb Zircon geochronology. Episodes 20, 188–192.
Li, Z., Li, X., 2007. Formation of the 1300-km-wide intracontinental orogen and postorogenic magmatic province in Mesozoic South China: a flat-slab subduction model. Geology 35, 179–182.
Li, X.-H., Sun, M., Wei, G.-J., Liu, Y., Lee, C.-Y., Malpas, L., 2000. Geochemical and Sm–Nd isotopic study of amphibolites in the Cathaysia Block, southeastern China: evidence for an extremely depleted mantle in the Paleoproterozoic. Precambrian Research 102, 251–262.
Li, W.-X., Li, X.-H., Li, Z.-X., Lou, F.-S., 2008. Obduction-type granites within the NE Jiangxi Ophiolite: implications for the final amalgamation between the Yangtze and Cathaysia Blocks. Gondwana Research 13, 288–301.
Li, X.-H., Li, W.-X., Li, Z.-X., Lo, C.-H., Wang, J., Ye, M.-F., Yang, Y.-H., 2009. Amalgamation between the Yangtze and Cathaysia Blocks in South China: constraints from SHRIMP U-Pb zircon ages, geochemistry and Nd-Hf isotopes of the Shuangxiwu volcanic rocks. Precambrian Research 174, 117–128.
Li, W.Y., Ma, C.Q., Liu, Y.Y., Robinson, P.T., 2012. Discovery of the Indosinian aluminum A-type granite in Zhejiang Province and its geological significance. Science China: Earth Sciences 55, 13–25.
Li, P., Yu, X., Li, H., Qiu, J., Zhou, X., 2013a. Jurassic–Cretaceous tectonic evolution of Southeast China: geochronological and geochemical constraints of Yanshanian granitoids. International Geology Review 55, 1202–1219.
Li, Z., Zhou, J., Mao, J., Santosh, M., Yu, M., Li, Y., Hu, Y., Langmuir, C.H., Chen, Z., Cai, X., Hu, Y., 2013b. Zircon U–Pb geochronology and geochemistry of two episodes of granitoids from the northwestern Zhejiang Province, SE China: implication for magmatic evolution and tectonic transition. Lithos 179, 334–352.
Li, J., Ma, Z., Zhang, Y., Dong, S., Li, Y., Lu, M.A., Tan, J., 2014a. Tectonic evolution of Cretaceous extensional basins in Zhejiang Province, eastern South China: structural and geochronological constraints. International Geology Review 56, 1602–1629.
Li, X., Zheng, J., Ma, Q., Xiong, Q., Griffin, W.L., Lu, J., 2014b. From enriched to depleted mantle: evidence from Cretaceous lamprophyres and Paleogene basaltic rocks in eastern and central Guangxi Province, western Cathaysia block of South China. Lithos 300–313.
Li, X., Zhu, P., Kusky, T.M., Gu, Y., Peng, S., Yuan, Y., Fu, J., 2015. Has the Yangtze craton lost its root? A comparison between the North China and Yangtze cratons. Tectonophysics 655, 1–14.
Liu, Y., Zong, K., Kelemen, P.B., Gao, S., 2008. Geochemistry and magmatic history of eclogues and ultramafic rocks from the Chinese continental scientific drill hole: subduction and ultrahigh-pressure metamorphism of lower crustal cumulates. Chemical Geology 247, 133–153.
Liu, Y., Gao, S., Hu, Z., Gao, C., Zong, K., Wang, D., 2010. Continental and Oceanic Crust Recycling-induced Melt-Peridotite Interactions in the Trans-North China Orogen: U–Pb Dating, Hf Isotopes and Trace Elements in Zircons from Mantle Xenoliths. J. Petrol. 51, 537–571.
Liu, C., Wu, F., Sun, J., Chu, Z., Qiu, Z., 2012. The Xinchang peridotite xenoliths reveal mantle replacement and accretion in southeastern China. Lithos 150, 171–187.
Liu, L., Xu, X., Zou, H., 2012a. Episodic eruptions of the Late Mesozoic volcanic sequences in southeastern Zhejiang, SE China: petrogenesis and implications for the geodynamics of paleo-Pacific subduction. Lithos 154, 166–180.
Liu, L., Qiu, J.S., Li, Z., Li, Y.L., 2012b. Petrogenesis of the Early Cretaceous quartz monzonite pluton at Muchen in Longyou County, Zhejiang Province: evidences from elemental and isotopic geochemistry of mafic microgranular encleaves and their host rocks. Acta Petrologica Sinica 28, 3993–4006.
Liu, L., Xu, X., Xia, Y., 2014a. Cretaceous Pacific plate movement beneath SE China: evidence from episodic volcanism and related intrusions. Tectonophysics 614, 170–184.
Liu, L., Qiu, J.S., Zhao, J.L., Yang, Z.L., 2014b. Geochronological, geochemical, and Sr–Nd–Hf isotopic characteristics of Cretaceous monzonitic plutons in western Zhejiang Province, Southeast China: new insights into the petrogenesis of intermediate rocks. Lithos 196–197, 242–260.
Liu, L., Qiu, J.-S., Zhao, J.-L., 2016. A hybrid origin for two Cretaceous monzonitic plutons in eastern Zhejiang Province, Southeast China: geochronological, geochemical, and Sr–Nd–Hf isotopic evidence. Journal of Asian Earth Sciences 115, 183–203.
Lu, J., Zheng, J., Griffin, W.L., Yu, C., 2013. Petrology and geochemistry of peridotite xenoliths from the Lianshan region: nature and evolution of lithospheric mantle beneath the lower Yangtze block. Gondwana Research 23, 161–175.
Ludwig, K.R., 2003. ISOPLOT 3.00: A Geochronological Toolkit for Microosoft Excel. Berkeley: Berkeley Geochronology Center. California.
Ma, Q., Zheng, J., Griffin, W.L., Zhang, M., Tang, H., Su, Y., Ping, X., 2012. Triassic “adakitic” rocks in an extensional setting (North China): melts from the cratonic lower crust. Lithos 149, 159–173.
Ma, Q., Xu, Y.-G., Zheng, J.-P., Griffin, W., Hong, L.-B., Ma, L., 2016. Coexisting Early Cretaceous High-Mg andesites and Adakitic rocks in the North China Craton: the role of water in intraplate magmatism and cratonic destruction. Journal of Petrology 57, 1279–1308.
Mao, J., Ye, H., Liu, K., Li, Z., Takahashi, Y., Zhao, X., Kee, W., 2013. The Indosinian collision–extension event between the South China Block and the Palaeo-Pacific plate: evidence from Indosinian alkaline granitic rocks in Dashuang, eastern Zhejiang, South China. Lithos 81–97.
McDonough, W.F., Sun, S.-s., 1995. The composition of the Earth. Chemical Geology 120, 223–253.
Meng, Q., Zhang, G., 1999. Timing of collision of the North and South China blocks: controversy and reconciliation. Geology 27, 123–126.
Menzies, M., 1993. Palaeozoic and Cenozoic lithoprobes and the loss of >120 km of Archaean Lithosphere Sino-Korean Craton China. Geological Society, London, Special Publications 76, 71–81.
Menzies, M.A., Xu, Y., Zhang, H., Fan, W., 2007. Integration of geology, geophysics and geochemistry: a key to understanding the North China Craton. Lithos 96, 1–21.
Moyen, J.-F., Stevens, G., 2006. Experimental Constraints on TTG Petrogenesis: Implications for Archean Geodynamics. Experimental constraints on TTG petrogenesis. pp. 149–175.
Niu, Y., 2005. Generation and evolution of basaltic magmas: some basic concepts and a hypothesis for the origin of the Mesozoic-Cenozoic volcanism in eastern China. Geological Journal of China Universities 11, 9–46.
Patiño Douce, A.E., 1996. Effects of pressure and H2O content on the compositions of primary crustal melts. Transactions of the Royal Society of Edinburgh: Earth Sciences 315, 11–21.
Patiño Douce, A.E., 1999. What do experiments tell us about the relative contributions of crust and mantle to the origin of granitic magmas? Geological Society, London, Special Publications 168, 55–75.
Qi, Y., Hu, R., Liu, S., Coulson, I.M., Qi, H., Tian, J., Zhu, J., 2016. Petrogenesis and geodynamic setting of Early Cretaceous mafic–ultramafic intrusions, South China: a case study from the Gan–Hang tectonic belt. Lithos 258–259, 149–162.
Qiu, J.-S., Wang, D.-Z., McInnes, B.I.A., Jiang, S.-Y., Wang, R.-C., Kanisawa, S., 2004. Two subgroups of A-type granites in the coastal area of Zhejiang and Fujian Provinces, SE China: age and geochemical constraints on their petrogenesis. In: Ishihara, S., Stephens, W.E., Harley, S.L., Arima, M., Nakajima, T. (Eds.), The Fifth Hutton Symposium on the Origin of Granites and Related Rocks. Transactions of the Royal Society of Edinburgh: Earth Sciences 95, pp. 227–236.
Rapp, R.P., Watson, E.B., 1995. Dehydration melting of metabasalt at 8–32 kbar: implications for continental growth and crust-mantle recycling. Journal of Petrology 36, 891–931.
Shen, W., Ling, H.-F., Wang, D., Xu, B., Yu, Y., 1999. Study on Nd–Sr isotopes of Mesozoic igneous rocks in Zhejiang, China. Scientia Geologica Sinica 34, 223–232.
Shui, T., 1988. Tectonic framework of the continental basement of southeast China. Scientia Sinica. Series B, Chemical, Biological, Agricultural, Medical & Earth Sciences 31, 885–896.
Sun, S., McDonough, W., 1989. Chemical and isotopic systematics of oceanic basalts: implications for mantle composition and processes. Geological Society, London, Special Publications 42, 313–345.
Sun, Y., Ma, C., Liu, Y., She, Z., 2011. Geochronological and geochemical constraints on the petrogenesis of late Triassic aluminous A-type granites in southeast China. Journal of Asian Earth Sciences 42, 1117–1131.

Sun, J., Liu, Z., Zhang, S., Li, X.G., Qi, J.F., 2017. Large-scale removal of lithosphere underneath the North China Craton in the Early Cretaceous: geochemical constraints from volcanic lavas in the Bohai Bay Basin. Lithos 292–293, 69–80.

Wang, Y.X., Zhao, Z.H., Bao, Z.W., Li, X.H., 1997. Geochemistry of granitoids from Zhejiang Province and crustal evolution–I. Phanerozoic granitoids. Geochimica 26, 1–15.

Weinberg, R.F., Hasalova, P., 2015. Water-fluxed melting of the continental crust: a review. Lithos 158–188.

Wiedenbeck, M., AllÉ, P., Corfu, F., Griffin, W., Meier, M., Oberli, F., Quadt, A.V., Roddick, J., Spiegel, W., 1995. Three natural zircon standards for U–Th–Pb, Lu–Hf, trace element and REE analyses. Geostand. Geoanal. Res. 19, 1–23.

Windley, B.F., Maruyama, S., Xiao, W.J., 2010. Delamination/thinning of sub-continental lithospheric mantle under Eastern China: the role of water and multiple subduction. American Journal of Science 310, 1250–1293.

Wong, J., Sun, M., Xing, G., Li, X.-h., Zhao, G., Wong, K., Yuan, C., Xia, X., Li, L., Wu, F., 2009. Geochemical and zircon U–Pb and Hf isotopic study of the Baijuhuajian metaluminous A-type granite: Extension at 125–100 Ma and its tectonic significance for South China. Lithos 112, 289–305.

Wong, J., Sun, M., Xing, G., Li, X.-h., Zhao, G., Wong, K., Wu, F., 2011. Zircon U–Pb and Hf isotopic study of Mesozoic felsic rocks from eastern Zhejiang, South China: geochemical contrast between the Yangtze and Cathaysia blocks. Gondwana Research 19, 244–259.

Wu, F., Jahn, B., Wilde, S.A., Sun, D.Y., 2000. Phanerozoic crustal growth: U ± Pb and Sr ± Nd isotopic evidence from the granites in northeastern China. Tectonophysics 328, 89–113.

Wu, F., Lin, J., Wilde, S.A., Zhang, X., Yang, J., 2005. Nature and significance of the Early Cretaceous giant igneous event in eastern China. Earth and Planetary Science Letters 233, 103–119.

Wu, F., Walker, R.J., Yang, Y., Yuan, H., Yang, J., 2006. The chemical-temporal evolution of lithospheric mantle underlying the North China Craton. Geochimica et Cosmochimica Acta 70, 5013–5034.

Wu, F., Han, R., Yang, J., Wilde, S.A., Zhai, M., Park, S., 2007. Initial constraints on the timing of granitic magmatism in North Korea using U-Pb zircon geochronology. Chemical Geology 238, 232–248.

Xiao, W., He, H., 2005. Early Mesozoic thrust tectonics of the northwest Zhejiang region (Southeast China). Geological Society of America Bulletin 117, 945–961.

Xiao, W., Windley, B.F., Hao, J., Zhai, M., 2003. Accretion leading to collision and the Permian Solonker suture, Inner Mongolia, China: termination of the central Asian orogenic belt. Tectonics 22.

Xu, Y., 2001. Thermo-tectonic destruction of the archaean lithospheric keel beneath the sino-korean craton in China: evidence, timing and mechanism. Physics and Chemistry of the Earth, Part A: Solid Earth and Geodesy 26, 747–757.

Xu, Y., 2014. Recycled oceanic crust in the source of 90–40 Ma basalts in North and Northeast China: evidence, provenance and significance. Geochimica et Cosmochimica Acta 143, 49–67.

Xu, X., Reilly, S.Y.O., Griffin, W.L., Zhou, X., 2000. Genesis of young lithospheric mantle in Southeastern China: an LAM–ICPMS trace element study. Journal of Petrology 41, 111–148.

Xu, Y., Hu, Y.H., Gu, M.G., Lu, C.Z., 2013. The tectonic extensional event during the Late Indosinian Period in the southeastern Zhejiang Province: evidence from the Dashuang pluton in Zhuji County. Acta Petrologica Sinica 29, 3131–3141.

Yan, J., Chen, J., Xu, X., 2008. Geochemistry of Cretaceous mafic rocks from the Lower Yangtze region, eastern China: characteristics and evolution of the lithospheric mantle. Journal of Asian Earth Sciences 33, 177–193.

Yang, S.-Y., Jiang, S.-Y., Zhao, K.-D., Jiang, Y.-H., Ling, H.-F., Luo, L., 2012. Geochronology, geochemistry and tectonic significance of two Early Cretaceous A-type granites in the Gan-Hang Belt, Southeast China. Lithos 150, 155–170.

Yu, X.Q., Shu, L.S., Yan, T.S., Yu, Y.W., Zu, F.P., Wang, B., 2004. Geochemistry of basalts of late period of Early Cretaceous from Jiangshan-Guangfeng, SE China and its tectonic significance. Geochimica 33, 465–476.

Yu, J., Oreilly, S.Y., Zhou, M., Griffin, W.L., Wang, L., 2012. U–Pb geochronology and Hf–Nd isotopic geochemistry of the Badu Complex, Southeastern China: implications for the Precambrian crustal evolution and paleogeography of the Cathaysia Block. Precambrian Research 222–223, 424–449.

Zhai, M., Fan, Q., Zhang, H., Sui, J., Shao, J., 2007. Lower crustal processes leading to Mesozoic lithospheric thinning beneath eastern North China: underplating, replacement and delamination. Lithos 96, 36–54.

Zhang, H., 2005. Transformation of lithospheric mantle through peridotite-melt reaction: a case of Sino-Korean craton. Earth and Planetary Science Letters 237, 768–780.

Zhang, H., Sun, M., Zhou, M., Fan, W., Zhou, X., Zhai, M., 2004. Highly heterogeneous Late Mesozoic lithospheric mantle beneath the North China Craton: evidence from Sr–Nd–Pb isotopic systematics of mafic igneous rocks. Geological Magazine 141, 55–62.

Zhang, S., Zhao, Y., Davis, G.A., Ye, H., Wu, F., 2014. Temporal and spatial variations of Mesozoic magmatism and deformation in the North China Craton: implications for lithospheric thinning and decratonization. Earth-Science Reviews 131, 49–87.

Zhang, J., Liu, Y., Ling, W., Gao, S., 2017. Pressure-dependent compatibility of iron in garnet: insights into the origin of ferropicritic melt. Geochimica et Cosmochimica Acta 197, 356–377.

Zhao, K., Jiang, S., Chen, W., Chen, P., Ling, H., 2013. Zircon U–Pb chronology and elemental and Sr–Nd–Hf isotope geochemistry of two Triassic A-type granites in South China: implication for petrogenesis and Indosinian transtensional tectonism. Lithos 292–306.

Zhao, L., Zhou, X., Zhai, M., Santosh, M., Ma, X., Shan, H., Cui, X., 2014. Paleoproterozoic tectonic transition from collision to extension in the eastern Cathaysia Block, South China: evidence from geochemistry, zircon U–Pb geochronology and Nd–Hf isotopes of a granite–charnockite suite in southwestern Zhejiang. Lithos 184–187, 259–280.

Zhao, L., Zhou, X., Zhai, M., Santosh, M., Geng, Y., 2015. Zircon U–Th–Pb–Hf isotopes of the basement rocks in northeastern Cathaysia block, South China: Implications for Phanerozoic multiple metamorphic reworking of a Paleoproterozoic terrane. Gondwana Research 28, 246–261.

Zhao, J.-L., Qiu, J.-S., Liu, L., Wang, R.-Q., 2016. The Late Cretaceous I- and A-type granite association of southeast China: implications for the origin and evolution of post-collisional extensional magmatism. Lithos 240, 16–33.

Zheng, J., Griffin, W.L., Reilly, S.Y.O., Yu, C., Zhang, H., Pearson, N.J., Zhang, M., 2007. Mechanism and timing of lithospheric modification and replacement beneath the eastern North China Craton: peridotitic xenoliths from the 100 Ma Fuxin basalts and a regional synthesis. Geochimica et Cosmochimica Acta 71, 5203–5225.

Zheng, J., Lee, C.A., Lu, J.G., Zhao, J., Wu, Y., Xia, B., Li, X.Y., Zhang, J.F., Liu, Y., 2015. Refertilization-driven destabilization of subcontinental mantle and the importance of initial lithospheric thickness for the fate of continents. Earth and Planetary Science Letters 409, 225–231.

Zhou, X.M., Li, W.X., 2000. Origin of Late Mesozoic igneous rocks in Southeastern China: implications for lithosphere subduction and underplating of mafic magmas. Tectonophysics 326, 269–287.

Zhou, X.-M., Sun, T., Shen, W.-Z., Shu, L.-S., Niu, Y.L., 2006. Petrogenesis of Mesozoic granitoids and volcanic rocks in south China: a response to tectonic evolution. Episodes 29, 26–33.

Zhu, R., Xu, Y., Zhu, G., Zhang, H., Xia, Q., Zheng, T., 2012. Destruction of the North China Craton. Science China: Earth Sciences 55, 1565–1587.